

UNIVERSITY OF THESSALY

DEPARTMENT OF MECHANICAL & INDUSTRIAL ENGINEERING

LABORATORY OF MECHANICS AND STRENGTH OF MATERIALS

Post-Graduate Diploma

Numerical Simulation of Mechanical Behavior
of Industrial Elbows

Patricia Pappa

Diploma in Mechanical and Industrial Engineering, University of Thessaly, 2006

Advisor: Dr. S.A. Karamanos

**Submitted to the Department of Mechanical
and Industrial Engineering
in Partial Fulfillment of the Requirements
for the Degree of Post-Graduate Diploma**

University of Thessaly, November 2008

ΠΑΝΕΠΙΣΤΗΜΙΟ ΘΕΣΣΑΛΙΑΣ

ΠΟΛΥΤΕΧΝΙΚΗ ΣΧΟΛΗ

ΤΜΗΜΑ ΜΗΧΑΝΟΛΟΓΩΝ ΜΗΧΑΝΙΚΩΝ ΒΙΟΜΗΧΑΝΙΑΣ

ΕΡΓΑΣΤΗΡΙΟ ΜΗΧΑΝΙΚΗΣ ΚΑΙ ΑΝΤΟΧΗΣ ΤΩΝ ΥΛΙΚΩΝ

Μεταπτυχιακή Εργασία

**Αριθμητική Προσωμοίωση της Μηχανικής
Συμπεριφοράς Βιομηχανικών Σωληνώσεων**

Πατρικία Παππά

Διπλωματούχου Μηχανολόγου Μηχανικού Βιομηχανίας Π.Θ., 2006

Επιβλέπων: Σ. Α. Καραμάνος

Υπεβλήθη για την εκπλήρωση μέρους των

απαιτήσεων για την απόκτηση του

Μεταπτυχιακού Διπλώματος Ειδίκευσης

Πανεπιστήμιο Θεσσαλίας, Νοέμβριος 2008



**ΠΑΝΕΠΙΣΤΗΜΙΟ ΘΕΣΣΑΛΙΑΣ
ΒΙΒΛΙΟΘΗΚΗ & ΚΕΝΤΡΟ ΠΛΗΡΟΦΟΡΗΣΗΣ
ΕΙΔΙΚΗ ΣΥΛΛΟΓΗ «ΓΚΡΙΖΑ ΒΙΒΛΙΟΓΡΑΦΙΑ»**

Αριθ. Εισ.: 7902/1
Ημερ. Εισ.: 12-09-2009
Δωρεά: Συγγραφέας
Ταξιθετικός Κωδικός: Δ
624.177
ΠΑΠ

©

Η έγκριση της μεταπτυχιακής εργασίας από το Τμήμα Μηχανολόγων Μηχανικών Βιομηχανίας της Πολυτεχνικής Σχολής του Πανεπιστημίου Θεσσαλίας δεν υποδηλώνει αποδοχή των απόψεων του συγγραφέα (Ν. 5343/32 αρ. 202 παρ. 2).

Εγκρίθηκε από τα Μέλη της Πενταμελούς Εξεταστικής Επιτροπής:

Πρώτος Εξεταστής (Επιβλέπων)	Δρ. Σπύρος Α. Καραμάνος Επίκουρος Καθηγητής, Τμήμα Μηχανολόγων Μηχανικών Βιομηχανίας, Πανεπιστήμιο Θεσσαλίας
Δεύτερος Εξεταστής	Δρ. Νικόλαος Αράβας Καθηγητής, Τμήμα Μηχανολόγων Μηχανικών Βιομηχανίας, Πανεπιστήμιο Θεσσαλίας
Τρίτος Εξεταστής	Δρ. Αλέξιος Κερμανίδης Λέκτορας, Τμήμα Μηχανολόγων Μηχανικών Βιομηχανίας, Πανεπιστήμιο Θεσσαλίας
Τέταρτος Εξεταστής	Δρ. Δημήτριος Σοφιανόπουλος Επίκουρος Καθηγητής, Τμήμα Πολιτικών Μηχανικών, Πανεπιστήμιο Θεσσαλίας
Πέμπτος Εξεταστής	Δρ. Γρηγόρης Χαϊδεμενόπουλος Καθηγητής, Τμήμα Μηχανολόγων Μηχανικών Βιομηχανίας, Πανεπιστήμιο Θεσσαλίας

Acknowledgments

I would like to express my sincerest gratitude to my advisor, Professor Spyros A. Karamanos, for his valuable support, guidance and friendship during the course of this research. Working with Professor Karamanos has been an important and interesting experience for me, a motive to always give my best, and one of the main reasons that made me pursue graduate studies.

I also feel obliged to thank the members of the examining committee, namely Professors N. Aravas, G. Haidemenopoulos, A. Kermanidis and D. Sofianopoulos for their valuable comments and suggestions.

At this point, I wish to express my sincere gratitude to the Public Benefit Foundation “Alexander S. Onassis” for the fellowships that awarded to me and facilitated greatly this work. These fellowships apart from the financial support constitute a great honor for me.

I’m grateful to my colleagues for their constant support scientifically and emotionally Dr. Sotiria Houliara, Thoma Dilmas, Daniel Vailikis, George Varelis and Aglaia Pournara.

Most of all, I’m grateful and indebted to my family for their encouragement and help and mainly constant love.

Patricia Pappa

In the memory of my grandfather

Table of Contents

Introduction	1
1.1 Structural behavior of pipe elbows and numerical simulation.....	1
1.2 Previous publications on ‘pipe’, ‘tube’ or ‘elbow’ elements	2
1.3 Scope of present study.....	4
“Tube Element” Description.....	5
2.1 Linear elasticity equations in curvilinear coordinates	5
2.2 Finite element discretization.....	8
2.3 “Tube element” description.....	10
Benchmark Numerical Results.....	17
3.1 Single – element tests	17
3.2 Element tests in a 90deg elbow	26
3.3 Elements tests on an industrial piping component	29
Numerical Results – Comparison with Experiments.....	34
4.1 Comparison with TNO experimental results.....	35
Conclusions	43
Appendix	44
References	48

Chapter 1

Introduction

1.1 Structural behavior of pipe elbows and numerical simulation

Curved pipe segments are widely used in pipelines and industrial piping. Because of the importance for safeguarding their structural integrity, much research has been devoted to the study of their mechanical behavior. It is well-known that the behavior of a tubular member under bending loads is characterized by a significant distortion of the cross-section. This distortion, often referred to as “ovalization” or “Brazier” effect, makes the tube more flexible and produces additional stresses, which need to be considered in analysis and design (Brazier, 1927). This phenomenon is more pronounced in curved pipes, referred to as “elbows” (Von Karman, 1911). Regular beam elements are inadequate to predict such a behavior, whereas the use of shell elements is often computationally expensive. The need for simple and efficient simulation of mechanical behavior of curved pipes has motivated the development of special-purpose elements, referred to as “pipe” or “elbow” or “tube” elements, as alternatives to shell elements. Those elements have been shown to be quite effective for modeling pipelines, elbows and piping systems. Among other advantages of those elements over shell elements, “pipe” elements are more convenient to apply boundary conditions and appropriate kinematic

constraints. Furthermore, the results from tube elements are more easily interpreted, in terms of longitudinal bending or cross-sectional distortion.

1.2 Previous publications on 'pipe', 'tube' or 'elbow' elements

Stress analysis of elbows and curved pipes has been subject of numerous theoretical and experimental studies. The pioneer work by von Karman (1911) presented the first analytical work on pipe bends subjected to in-plane bending. The analysis was derived by superimposing pipe section ovalization on curved beam theory displacements. Von Karman's analysis was extended by Vigness (1943) for out-of-plane bending. Rodabaugh and George (1957) extended the above works, presenting a unifying approach for in-plane and out-of-plane elbow behavior, though the use of doubly-symmetric trigonometric functions. Furthermore Dodge and Moore (1972) proposed a simple approach for linear analysis of pipes bends based on the solution of Rodabaugh and George (1957), which is widely used in engineering design.

All the above theoretical analyses are limited because of the various assumptions and approximations made in formulation of the problem. Owing to limitations and difficulties in the foregoing analysis, it would be useful to employ a general approach that would be able to model pipe bends with different geometries, end constraints and various loading conditions. The finite element method represents a rigorous and general approach for the solution of elbow mechanics problems. Towards this purpose, special-purpose finite element formulations have been developed as alternatives to more rigorous shell element formulations. Bathe and Almeida (1980, 1982) presented a pipe elbow element that is simple and effective. The element was based on the classical von Karman solution of elbow bending, and uses a simplified version of linear ring theory for cross-sectional ovalization. The works of Bathe & Almeida were the first (a) to distinguish longitudinal (beam-type) deformation from cross-sectional ovalization and (b) to combine them in a simple and efficient manner. Note that ovalization was assumed to be in-plane (no-warping)

and inextensional, whereas a series of trigonometric functions was employed to discretize in-plane displacements (radial and tangential).

Militello & Huespe (1988) proposed a further improvement of the above element considering including warping deformation, but keeping the inextensionality condition. Hermite polynomials were used to ensure inter-element continuity. In a more recent paper, Yan et al. (1999) have proposed an “enhanced pipe elbow element”, which further improves the above concepts and capabilities. Their element allowed for warping deformation, and accounted for a certain degree of cross-sectional extentionality and for non-symmetric cross-sectional deformation. Moreover, Yan et al. (1999) considered the contribution of pressure on the stiffness matrix (i.e. the “pressure stiffness”). Their element was used for the limit plastic analysis of tubes, using a mathematical programming technique. Hibbit et al. (1999) presented an elbow element for the elastic and elastic-plastic analysis of initially straight and bent tubes under pressure and structural loads, incorporated in the finite element program Abaqus. The element is based on the Koiter – Sanders linear shell kinematics and on a discrete Kirchhoff concept, imposed through a penalty formulation. Cross-sectional warping is included and the corresponding deformation parameters are discretized through the use of trigonometric functions up to the 6th degree.

In addition to above analytical works, numerous experimental works have been reported. Sobel and Newman (1980, 1986) and Dhalla (1987) reported experimental data of stress and strain around the elbow cross-section and along the pipe, on the elastic-plastic bending response of elbows, through a series of tests on 16-in 90 deg elbows ($D/t=39$ and $R/r=3$) under in-plane closing moments. The experimental results were compared with the numerical from simplified elbow elements. Gresnigt et al. (1985, 1986, 1996) reported test results on 30 deg and 60 deg elbows ($R/r=6$) under in-plane bending, and reported moment-curvature curves, variations of ovalization along the length. Those tests are examined in detail in the present work, and compared with numerical results. Hilsenkopf et al. (1988) conducted tests on

thin-walled ($D/t=89.5$) stainless steel elbows and thick-walled ($D/t=13.4$) ferritic elbows under both in-plane and out-of-plane bending, in connection with their functional capability. In-plane bending experiments on 90 deg elbows were reported by Suzuki and Nasu (1989) and, more recently, by Tan et al. (2002). In both works, the test results were compared with finite element results.

1.3 Scope of present study

In the present study, the development of a family of continuum-type tube elements is described. The elements are aimed at providing simple and efficient stress analysis of pipes and elbows towards a reliable engineering design. A three-node version of the “tube element” was first developed by Karamanos and Tassoulas (1996) for the nonlinear analysis of relatively thick inelastic tubes. Later this element was employed for the buckling analysis of thin-walled elastic cylinders. Herein, a family of such elements is developed and tested in standard benchmark problems, in terms of their accuracy and computational efficiency.

For each element of the proposed element family (2-node, 3-node, 4-node), a series of studies are conducted to determine its optimum behavior. The basic issues to be examined are the number of cross-sectional parameters and the number of integration points in the three directions within the pipe. Several benchmark problems are used towards this purpose. Comparisons are made with analytical solutions and shell-elements, in terms of the corresponding strain and stress distributions. Finally, a comparison with available experimental data from TNO, the Netherlands, is also conducted.

Chapter 2

“Tube Element” Description

In this chapter, the background theory of this work is presented. A linear finite element technique is adopted, based on the Lagrangian description of the tube as an linear elastically deforming continuum. The development of a family of “tube elements” is presented, which are able to predict accurately the deformation and stress stage in curved pipe segments. In an early paper a three-node version of this element, has been developed by Karamanos and Tassoulas (1996). The formulation adopts a linear elasticity formulation in curvilinear coordinates. Some basic concepts necessary for the development of theoretical formulation, as well as the numerical implementation of the formulation, are presented in the following.

2.1 Linear elasticity equations in curvilinear coordinates

The material behavior is described through a linear elastic material model for infinitesimal deformations. The fundamental problem of elasticity can be described by the three groups of the basic equations, namely kinematics, constitutive equations and equilibrium. Linear kinematic equations, relate the strain tensor to the symmetric part of the displacement vector gradient, and can be written as

$$\boldsymbol{\varepsilon} = \text{symm}[\nabla \mathbf{u}] \quad (2.1)$$

where \mathbf{u} is the vector of the displacements and $\nabla \mathbf{u}$ is the displacement gradient tensor. The constitutive equations

$$\boldsymbol{\sigma} = [\mathcal{D}] \boldsymbol{\varepsilon} \quad (2.2)$$

where $[\mathcal{D}]$ is the fourth order elastic rigidity tensor and $\boldsymbol{\sigma}$ is the stress tensor. Finally the equilibrium equations

$$\text{div}(\boldsymbol{\sigma}) + \rho \mathbf{b} = 0 \quad (2.3)$$

relate the stresses $\boldsymbol{\sigma}$ with the forces per unit volume \mathbf{b} and ρ is the density.

The tube is described as isotropic elastic continuum using curvilinear coordinates. These coordinates are denoted by ξ^i ($i=1,2,3$), where \mathbf{g}_k are the covariant base vectors and \mathbf{g}^k are the contravariant base vectors, the above kinematic equations can be rewritten as

$$\varepsilon_{kl} = \frac{1}{2} (u_{k/l} + u_{l/k}) \quad (2.4)$$

where standard index notation is adopted, and

$$\boldsymbol{\varepsilon} = \varepsilon_{kl} (\mathbf{g}^k \otimes \mathbf{g}^l) \quad (2.5)$$

In the above equation (2.4), $u_{k/l} = \frac{\partial \mathbf{u}}{\partial \xi^l} \cdot \mathbf{g}_k$ are the components of the covariant derivative of the displacement vector. The constitutive relations, using the curvilinear coordinates, are expressed as

$$\boldsymbol{\sigma}^{ij} = \mathcal{D}^{ijkl} \varepsilon_{kl} \quad (2.6)$$

where

$$\boldsymbol{\sigma} = \sigma^{ij} (\mathbf{g}_i \otimes \mathbf{g}_j) \quad (2.7)$$

and the components \mathcal{D}^{ijkl} of the elastic rigidity fourth-order tensor have the following form for isotropic behavior

$$\mathcal{D}^{ijkm} = \frac{E}{2(1+\nu)} \left[(g^{ik} g^{jl} + g^{jk} g^{il}) + \frac{2\nu}{1-2\nu} g^{ij} g^{kl} \right] \quad (2.8)$$

In the above expression, the physical parameters E , ν are the Young's modulus and the Poisson's ratio respectively. These "engineering" constants can be expressed through the so-called Lamé constants denoted λ and μ , which are defined as follows

$$\lambda = \frac{E\nu}{(1+\nu)(1-2\nu)} \quad (2.9)$$

$$\mu = \frac{E}{2(1+\nu)} \quad (2.10)$$

The equilibrium equations, using the vector and tensor components in the curvilinear coordinates, can be written

$$\text{div} \left[\sigma^{ij} (g_i \otimes g_j) \right] + \rho b^k g_k = 0 \quad (2.11)$$

and in component form

$$\sigma^{ij}_{i/j} + \rho b^i = 0 \quad (2.12)$$

Equilibrium is expressed through the principle of virtual work, considering an admissible displacement field $\delta \mathbf{u}$. This means that $\delta \mathbf{u} = 0$ in B_u , where B_u is the part of boundary B where kinematic boundary conditions exist. The principle of virtual work, is expressed as

$$\int_V \boldsymbol{\sigma} \cdot (\nabla \delta \mathbf{u}) dV = \int_{B_q} \mathbf{t} \cdot \delta \mathbf{u} dB_q \quad (2.13)$$

and with contravariant components

$$\int_V \sigma^{ij} \delta u_{i/j} dV = \int_{B_q} t^k \delta u_k dB_q \quad (2.14)$$

where V and B_q are the volume and boundary surface of the body, respectively, σ^{ij} are the contravariant components of the true stress with respect to the basis $\mathbf{g}_i \otimes \mathbf{g}_j$, \mathbf{t} is the traction vector on the boundary and $\delta u_{i/j}$ are the covariant components of the gradient of $\delta \mathbf{u}$, defined as

$$\delta u_{i/j} = \frac{\partial(\delta \mathbf{u})}{\partial \xi^j} \cdot \mathbf{g}_i \quad (2.15)$$

2.2 Finite element discretization

The numerical technique applied in this study relies on the principle of virtual work. Using Galerkin's approximation method through appropriate shape functions N_i , the incremental displacement field can be written as

$$\mathbf{u} = [\mathbf{N}] \hat{\mathbf{U}} \quad (2.16)$$

in which $[\mathbf{N}]$ is the interpolation matrix that contains shape functions N_i and $\hat{\mathbf{U}}$ contains the nodal degrees of freedom (e.g. displacements and rotations). According to the standard Galerkin method the same functions are also used for discretizing the virtual displacements, so that

$$\delta \mathbf{u} = [\mathbf{N}] \delta \hat{\mathbf{U}} \quad (2.17)$$

The covariant differentiation of equations (2.16) and (2.17) results in:

$$\text{grad}(\mathbf{u}) = \{u_{k/i}\} = [\mathbf{B}] \hat{\mathbf{U}} \quad (2.18)$$

$$\text{grad}(\delta \mathbf{u}) = \{\delta u_{k/i}\} = [\mathbf{B}] \delta \hat{\mathbf{U}} \quad (2.19)$$

where $[\mathbf{B}]$ contains the derivatives of the elements of the interpolation matrix.

Furthermore, the traction component normal to any shell lamina is imposed to be zero, following classical shell theory. The unit vector normal to the lamina, in the

current configuration is $\mathbf{g}^3 / \|\mathbf{g}^3\|$. Therefore the track in component normal to the lamina is $(\boldsymbol{\sigma} \mathbf{g}^3) \cdot \mathbf{g}^3$, and this leads to $\sigma^{33} = 0$.

On account of the symmetry of the stress, and because $\sigma^{33} = 0$, a 5-element column vector of stress components σ^{ij} is considered as

$$\boldsymbol{\sigma} = \begin{bmatrix} \sigma^{11} \\ \sigma^{22} \\ \sigma^{12} \\ \sigma^{23} \\ \sigma^{31} \end{bmatrix} \quad (2.20)$$

and similarly, the column vector of strain components is written as

$$\boldsymbol{\varepsilon} = \begin{bmatrix} \varepsilon_{11} \\ \varepsilon_{22} \\ \varepsilon_{12} \\ \varepsilon_{23} \\ \varepsilon_{31} \end{bmatrix} \quad (2.21)$$

Furthermore from equation (2.2), a 5x5 constitutive matrix $[\boldsymbol{\mathcal{D}}]$ can be written. On the basis of the symmetry of the components D^{ijpq} , it can be shown that $[\boldsymbol{\mathcal{D}}]$ is a symmetric matrix. The covariant derivatives of displacement components can be written in a 9-element column vector as follows

$$\{\mathbf{u}_{p/q}\} = \begin{bmatrix} u_{1/1} \\ u_{2/1} \\ u_{3/1} \\ u_{1/2} \\ u_{2/2} \\ u_{3/2} \\ u_{1/3} \\ u_{2/3} \\ u_{3/3} \end{bmatrix} \quad (2.22)$$

A 5x9 matrix $[\mathbf{W}]$ containing these components is also introduced, so that

$$[\mathbf{W}] = \begin{bmatrix} 1 & 0 & 0 & 0 & 0 & 0 & 0 & 0 & 0 \\ 0 & 0 & 0 & 0 & 1 & 0 & 0 & 0 & 0 \\ 0 & 1 & 0 & 1 & 0 & 0 & 0 & 0 & 0 \\ 0 & 0 & 0 & 0 & 0 & 1 & 0 & 1 & 0 \\ 0 & 0 & 1 & 0 & 0 & 0 & 1 & 0 & 0 \end{bmatrix} \quad (2.23)$$

expressing equation (2.4). Therefore, the equilibrium equations of the element assemblage corresponding to the nodal point displacements are

$$[\mathbf{K}]\hat{\mathbf{U}} = \mathbf{F} \quad (2.24)$$

where $[\mathbf{K}]$ is the incremental stiffness matrix

$$[\mathbf{K}] = \int_{V_0} [\mathbf{B}]^T [\mathbf{W}]^T [\mathcal{D}] [\mathbf{W}] [\mathbf{B}] dV_0 \quad (2.25)$$

and \mathbf{F} is the load vector.

After assembling the stiffness matrices and load vectors of all elements, using the above relations, the system of equations for the displacements $\hat{\mathbf{U}}$ is solved and the state of stress and strain are obtained.

2.3 “Tube element” description

The linear “tube element” is presented in this section, which is employed for simulating the behavior of elbows subjected to bending within the plane of the elbow. This element combines longitudinal (beam-type) with cross-sectional deformation (ovalization) in an efficient manner. The geometry and displacements are interpolated using polynomials in the longitudinal direction while Fourier series expansions are used at each nodal cross section. A Cartesian coordinate system is used, where the x_3 -axis is in the longitudinal direction. Symmetry of the tube is assumed with respect to the x_2 - x_3 plane, and therefore, the position and orientation of the cross section at each node (k) is defined through three nodal degrees of freedom, two translational ($u_2^{(k)}$ and $u_3^{(k)}$ in the direction of x_2 and x_3 axes

respectively) and one rotational ($\theta_1^{(k)}$ about x_1 axis). Figure 1 shows the 3-node version of the tube element.

The deformed tube axis is defined by

$$\mathbf{x}_c(\zeta) = \sum_{k=1}^{NNE} N^{(k)}(\zeta) \mathbf{x}^{(k)} \quad (2.26)$$

where $\mathbf{x}^{(k)}$ is the position vector of node (k), $N^{(k)}(\zeta)$ is the corresponding Lagrangian interpolation function and NNE is the number of nodes per element. In the present work three versions of this element family are considered, with two, three and four nodes (NNE=2, 3, 4). The corresponding Lagrangian functions for each tube element type (2-node, 3-node, 4-node), are linear, quadratic or cubic polynomials.

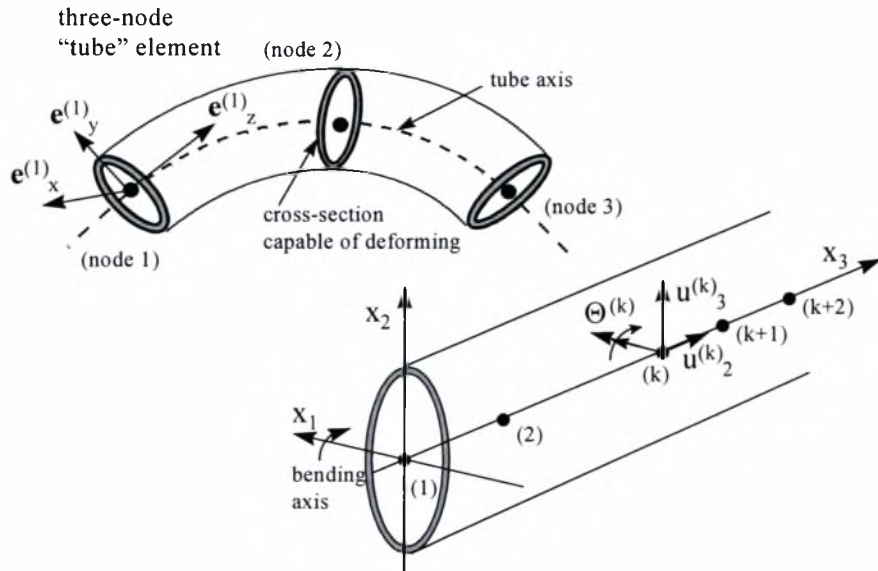


Figure 1: A three-node tube element and deformation parameters; $x_2 - x_3$ is the plane of bending.

To describe cross-sectional deformation, thickness is assumed to be constant and a reference line is chosen within the cross-section.

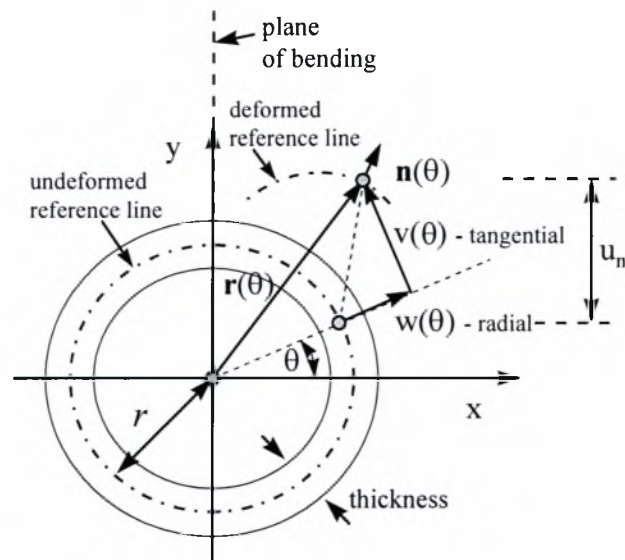


Figure 2: Cross-sectional ovalization (in-plane) deformation parameters.

Two types of cross-sectional deformation exist, in-plane deformation (ovalization) and out-of-plane (warping). For in-plane deformation, fibers initially normal to the reference line remain normal to the reference line.

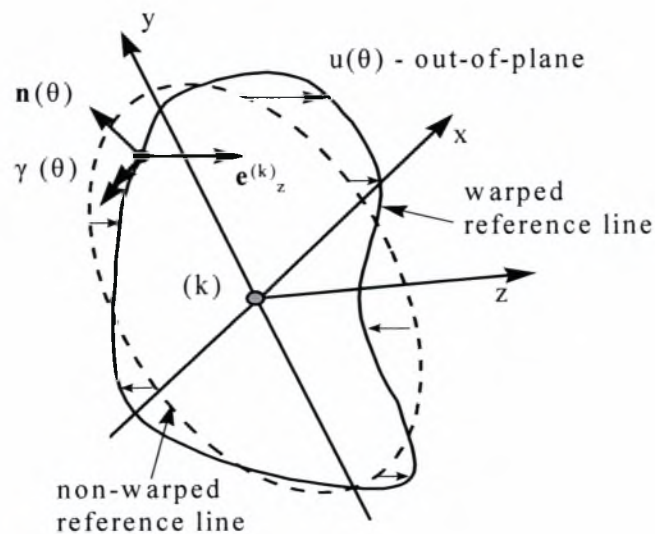


Figure 3: Cross-sectional warping (out-of-plane) deformation parameters.

The position of the reference line at the cross-section with the respect to node (k) is

$$\mathbf{r}^{(k)}(\theta) = x_r(\theta)\mathbf{e}_x^{(k)} + y_r(\theta)\mathbf{e}_y^{(k)} + z_r(\theta)\mathbf{e}_z^{(k)} \quad (2.27)$$

where x_r , y_r and z_r are reference line coordinates with respect to the local cross-section axes. The outward unit vector $\mathbf{n}^{(k)}(\theta)$, normal to the reference line can be written in terms of the position vector of reference line:

$$n_x = -\frac{1}{r} \frac{dy_r}{d\theta} \quad (2.28)$$

$$n_y = \frac{1}{r} \frac{dx_r}{d\theta} \quad (2.29)$$

The position vector of an arbitrary point at the initial configuration is

$$\mathbf{x}(\theta, \zeta, \rho) = \sum_{k=1}^{NNE} \left[\left(\mathbf{x}^{(k)} + \mathbf{r}_0^{(k)}(\theta) + \rho \mathbf{n}_0^{(k)}(\theta) \right) N^{(k)}(\zeta) \right] \quad (2.30)$$

where $\mathbf{r}_0^{(k)}$ is the position of the reference line in the initial configuration

$$\mathbf{r}_0^{(k)}(\theta) = x_0^r(\theta)\mathbf{e}_x^{(k)} + y_0^r(\theta)\mathbf{e}_y^{(k)} + z_0^r(\theta)\mathbf{e}_z^{(k)} \quad (2.31)$$

with components

$$\begin{aligned} x_r^0(\theta) &= r \cos \theta \\ y_r^0(\theta) &= r \sin \theta \\ z_r^0(\theta) &= 0 \end{aligned} \quad (2.32)$$

and $\mathbf{n}_0^{(k)}(\theta)$ is the outward normal unit vector in the initial configuration, with components

$$\begin{aligned} n_x^0 &= \cos \theta \\ n_y^0 &= \sin \theta \end{aligned} \quad (2.33)$$

Differentiating the position vector with respect to the local coordinates of the position vector as follows

$$\mathbf{g}_1 = \mathbf{g}_\theta = \frac{\partial \mathbf{x}}{\partial \theta} = \sum_{k=1}^{NNE} \left[\left(\frac{\mathbf{r}_0^{(k)}(\theta)}{d\theta} + \rho \frac{\mathbf{n}_0^{(k)}(\theta)}{d\theta} \right) N^{(k)}(\zeta) \right] \quad (2.34)$$

$$\mathbf{g}_2 = \mathbf{g}_\zeta = \frac{\partial \mathbf{x}}{\partial \zeta} = \sum_{k=1}^{NNE} \left[\left(\mathbf{x}^{(k)} + \mathbf{r}_0^{(k)}(\theta) + \rho \mathbf{n}_0^{(k)}(\theta) \right) \frac{N^{(k)}(\zeta)}{d\zeta} \right] \quad (2.35)$$

$$\mathbf{g}_3 = \mathbf{g}_\rho = \frac{\partial \mathbf{x}}{\partial \rho} = \sum_{k=1}^{NNE} \left[\left(\mathbf{n}_0^{(k)}(\theta) \right) N^{(k)}(\zeta) \right] \quad (2.36)$$

The displacement of the relative position of the reference line is

$$\begin{aligned} \Delta x_r &= (\cos \theta) w + (-\sin \theta) v \\ \Delta y_r &= (\sin \theta) w + (\cos \theta) v \\ \Delta z_r &= u \end{aligned} \quad (2.37)$$

where w , v are the radial and tangential displacement of the reference line at a certain node (k), and u is the out-of-plane warping displacement. Furthermore, the change of the outward in-plane normal vector due to cross-sectional deformation is

$$\begin{aligned} \Delta n_x &= n_x - n_x^0 = \left(\frac{w' - v}{r} \right) \sin \theta \\ \Delta n_y &= n_y - n_y^0 = \frac{v - w'}{r} \cos \theta \end{aligned} \quad (2.38)$$

where prime ($'$) denotes differentiation with respect to θ .

Therefore, the displacement vector of an arbitrary point in the elbow can be written as follows

$$\begin{aligned} \mathbf{u}(\theta, \zeta, \rho) &= \sum_{k=1}^{NNE} [(\mathbf{u}^{(k)} + (\Delta x_r + \rho \Delta n_x) \mathbf{e}_x^{(k)} + (\Delta y_r + \rho \Delta n_y) \mathbf{e}_y^{(k)} \\ &\quad + (y_r + \rho n_y) \theta^{(k)} \mathbf{e}_z^{(k)} + (u + \rho \gamma) \mathbf{e}_z^{(k)}) N^{(k)}(\zeta)] \end{aligned} \quad (2.39)$$

Furthermore, for the purposes of applying equation (2.4) differentiation of the displacement vector \mathbf{u} is conducted as follows

$$\mathbf{u}_{,1} = \frac{\partial \mathbf{u}}{\partial \theta} = \sum_{K=1}^{NNE} \left[(\Delta x'_r + \rho \Delta n'_x) \mathbf{e}_x^{(k)} + (\Delta y'_r + \rho \Delta n'_y) \mathbf{e}_y^{(k)} + (u'_z + \rho \gamma') \mathbf{e}_z^{(k)} + (y'_r + \rho n'_y) \Delta \theta \mathbf{e}_z^{(k)} \right] N^{(k)}(\zeta) \quad (2.40)$$

$$\mathbf{u}_{,2} = \frac{\partial \mathbf{u}}{\partial \zeta} = \sum_{K=1}^{NNE} \left[\mathbf{u}^{(k)} + (\Delta x_r + \rho \Delta n_x) \mathbf{e}_x^{(k)} + (\Delta y_r + \rho \Delta n_y) \mathbf{e}_y^{(k)} + (u + \rho \gamma) \mathbf{e}_z^{(k)} + (y_r + \rho n_y) \Delta \theta \mathbf{e}_z^{(k)} \right] \frac{dN^{(k)}}{d\zeta} \quad (2.41)$$

$$\mathbf{u}_{,3} = \frac{\partial \mathbf{u}}{\partial \rho} = \sum_{K=1}^{NNE} \left[\Delta n_x \mathbf{e}_x^{(k)} + \Delta n_y \mathbf{e}_y^{(k)} + n_y \theta \mathbf{e}_z^{(k)} + \gamma \mathbf{e}_z^{(k)} \right] N^{(k)}(\zeta) \quad (2.42)$$

Finally, the displacements $w(\theta)$, $v(\theta)$, $u(\theta)$ and the out-of-plane (warping) rotation $\gamma(\theta)$ at each cross-section are discretized using the trigonometric functions:

$$\begin{aligned} w(\theta) &= a_0 + a_1 \sin \theta + \sum_{n=2,4,6,\dots} a_n \cos n\theta + \sum_{n=3,5,7,\dots} a_n \sin n\theta \\ v(\theta) &= -a_1 \sin \theta + \sum_{n=2,4,6,\dots} b_n \sin n\theta + \sum_{n=3,5,7,\dots} b_n \cos n\theta \\ u(\theta) &= \sum_{n=2,4,6,\dots} c_n \cos n\theta + \sum_{n=3,5,7,\dots} c_n \sin n\theta \\ \gamma(\theta) &= \gamma_0 + \sum_{n=2,4,6,\dots} \gamma_n \cos n\theta + \sum_{n=1,3,5,7,\dots} \gamma_n \sin n\theta \end{aligned} \quad (2.43)$$

which are symmetric with respect to the $(-\pi/2 \leq \theta \leq \pi/2)$ line. Coefficients a_n , b_n refer to in-plane cross-sectional deformation (“ovalization” parameters) and c_n , γ_n refer to out-of-plane cross-sectional deformation (“warping” parameters). In the above expressions, symmetry with respect to the x_2 - x_3 plane is considered because of in-plane bending and only half of the tube is analyzed $(-\pi/2 \leq \theta \leq \pi/2)$.

Coefficients a_n , b_n , c_n , γ_n are degrees of freedom at each node (k), in addition to the two displacement $u_2^{(k)}$, $u_3^{(k)}$ and the rotation $\theta^{(k)}$. For every element, the column vector $\hat{\mathbf{U}}$ contains the degrees of freedom is defined as

$$\left\{\hat{\mathbf{U}}\right\}=\left[\cdots \quad \mathbf{u}_2^{(k)} \quad \mathbf{u}_3^{(k)} \quad \theta_1^{(k)} \quad \cdots \quad \mathbf{a}_i^{(k)} \quad \cdots \quad \mathbf{b}_i^{(k)} \quad \cdots \quad \gamma_i^{(k)} \quad \cdots \quad \mathbf{c}_i^{(k)} \quad \cdots\right]^T \quad (2.44)$$

and the matrices $[N]$ and $[B]$ are readily defined.

Chapter 3

Benchmark Numerical Results

Numerical results are obtained for the stress and deformation of curved tubes, under bending loads are conducted. For each element of the proposed “tube element family” (2-node, 3-node, 4-node), a series of studies are conducted in order to determine its optimum behavior. The basic issues examined are the optimum number of cross-sectional parameters and the corresponding number of integration points in the three directions. Several benchmark problems are considered towards this purpose, and comparisons analytical solutions are conducted, in terms of the pipe deformation and stresses.

3.1 Single – element tests

Different elements from the tube element family (2-node, 3-node and 4-node) are implemented, and a series of studies in elastic curved pipe segments are examined under bending, in order to determine their optimum behavior.

In-plane behavior of elastic curved pipe segments is examined. The numerical results are compared with analytical solution developed through a simple energy formulation to describe the ovalization (two-dimensional) behavior of elastic elbows. This solution, briefly described in the Appendix, has been presented by Rodabaugh and George (1957), and constitutes a generalization of the classical Von Karman

solution for non-pressurized pipe elbows (Von Karman, 1911). In this formulation, assuming uniform cross-sectional deformation along the elbow axis, the total potential energy of the bend elbow is expressed in terms of the radial and the tangential displacements, denoted w , v respectively. Those displacements are discretized through series of doubly-symmetric trigonometric functions. Solution is obtained by minimization of the potential energy, and is expressed in terms of the flexibility factor, which expresses the ratio of elbow flexibility over the flexibility of a straight pipe of equal length and of the same cross-section. Furthermore, the longitudinal and hoop stresses, the normalized curvature κ and the ovalization of the cross-section are also computed.

An infinitely long curved pipe is considered under bending. Under such conditions uniform deformation and stress exist along the pipe allowing for a two-dimensional analysis. To conduct a two-dimensional (ovalization) analysis, a slice is considered. The slice is very small in the longitudinal direction. The response of initially curved segment (Figure 4) is analyzed for elements with different number of nodes (2 nodes-3nodes-4nodes) in the element. Subsequently, a parametric study is conducted to investigate the response of slice (2 degrees) in terms of the order of Fourier expansion. The outside diameter is 165 mm and the thickness is 3 mm, and R is equal to 480 mm. A bending moment is equal to 10 kN-m and, the Young's modulus and Poisson's ratio are $E=210$ GPa and $\nu=0.3$ respectively. The elbow geometry can be expressed in terms of the dimensionless elbow parameter λ , defined

$$\lambda = \frac{tR}{r^2 \sqrt{1-\nu^2}} \quad (3.1)$$

which is equal to 0.23 for our case. The ovalization of elbow cross-section is expressed in terms of the ovalization parameter

$$ov = \frac{|D_h - D_v|}{2D_m} \quad (3.2)$$

where D_h and D_v are the deformed lengths of the horizontal diameter (normal to the plane of bending) and of the vertical diameter (on the plane of bending) and D_m is the mean tube diameter. The curvature k is defined as

$$k = \frac{\Delta\alpha}{L} \quad (3.3)$$

where $\Delta\alpha$ is the relative rotation between the ends of the curved pipe segment and $L = R\alpha$ (Figure 4) and is normalized by the curvature-like parameter $k_N = t/(r^2\sqrt{1-\nu^2})$, so that $\kappa = k/k_N$.

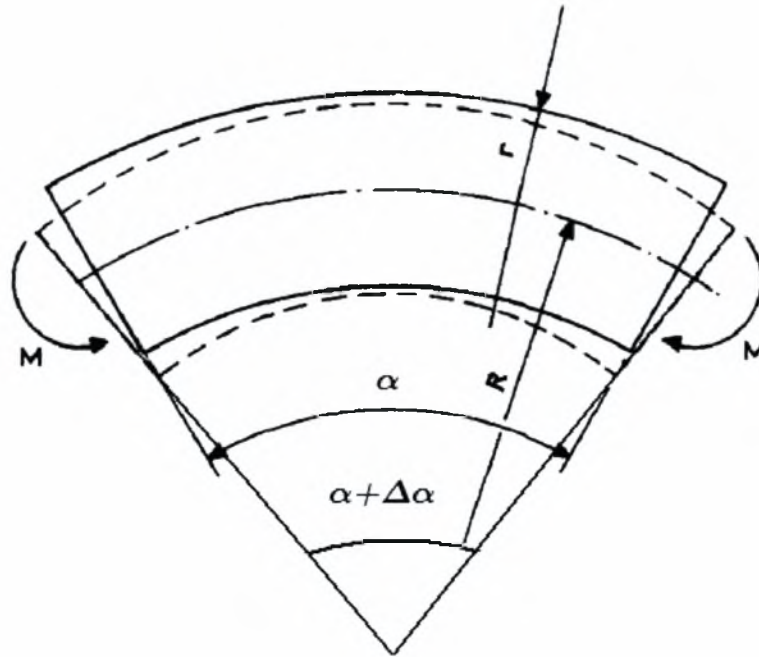


Figure 4: Configuration of elbow “slice” used for the parametric study.

This two-dimensional analysis is conducted with only one “tube element” in the longitudinal direction, using appropriate “symmetry” conditions at the two ends, which enforce all cross-sections to exhibit the same deformation without warping. Trigonometric functions up to 10th degree are considered for this analysis. The numbers of integration points in the three directions are the optimum for the computations, an issue to be determined in a later paragraph of the present chapter.

A first study concerns the determination of the number of Fourier coefficients for the ovalization a_n , b_n parameters, necessary for obtaining accurate results. Note that warping c_n , γ_n are not activated in the present analysis. The ovalization of the slice is presented for 2-node “tube element” in Table 1. Similarly, tables 2 and 3 present the ovalization of the elbow using the 3-node and the 4-node “tube element” respectively. Since the behavior is purely cross-sectional (two-dimensional), all elements exhibit similar behavior.

Number of Fourier	Ovalization
4	0.039384
6	0.039665
8	0.039668
10	0.039668
Analytical solution	0.039820



Table 1: Ovalization of slice; comparison of analytical solution with numerical results, for 2- node “tube element”.

Number of Fourier	Ovalization
4	0.039383
6	0.0396644
8	0.039667
10	0.039667
Analytical solution	0.039820

Table 2: Ovalization of slice; comparison of analytical solution with numerical results, for 3-node “tube element”.

Number of Fourier	Ovalization
4	0.039383
6	0.039664
8	0.039667
10	0.039667
Analytical solution	0.039820

Table 3: Ovalization of slice; comparison of analytical solution with numerical results, for 4-node “tube element”.

Convergence of the results is verified by increasing the number of terms in the trigonometric series until the required accuracy was achieved. The results show that an 8th degree expansion is necessary to provide satisfactory convergence. In those analyses, equally-spaced integration points are used (trapezoidal rule). The optimum number of integration points is examined below.

For the evaluation of the element stiffness matrix and force vector that corresponds to the current element stresses numerical integration is used. An important consideration is the minimum number of integration points required for the evaluation of the integral in equation (2.24). A parametric study is conducted to determine the number of integration points around the half-circumference that are necessary for this analysis. Linear interpolation is assumed in the radial direction (through the thickness) and, therefore, for the case of elastic behavior, exact integration requires two integration points. Finally, the number of integration points in the longitudinal direction is inconsequential because of the two-dimensional nature of the problem. The ovalization of the cross-section is presented for 2-node “tube element” in Table 4. Similarly, Table 5 and Table 6 present the ovalization of the slice for 3-node and 4-node “tube element” respectively.

Number of integration points around half-circumference	Ovalization
5	44.379469
7	0.085104
9	0.039668
11	0.039668
13	0.039668
Analytical solution	0.039820

Table 4: Ovalization of slice; comparison of analytical solution with numerical results, for 2-node “tube element” and trigonometric expansions 8th degree.

Number of integration points around half-circumference	Ovalization
5	44.435160
7	0.085121
9	0.039667
11	0.039667
13	0.039667
Analytical solution	0.039820

Table 5: Ovalization of slice; comparison of analytical solution with numerical results, for 3-node “tube element” and trigonometric expansions 8th degree.

Number of integration points around half-circumference	Ovalization
5	44.435172
7	0.085098
9	0.039667
11	0.039667
13	0.039667
Analytical solution	0.039820

Table 6: Ovalization of slice; comparison of analytical solution with numerical results, for 4-node “tube element” and trigonometric expansions 8th degree.

The results show that 9 equidistant points around the half-circumference, i.e. 17 points around the entire circumference, are necessary for “exact” integration. Suppose that trigonometric expansions up to degree n are used. This means that the stiffness matrix will contain terms up to degree $2n$. Therefore, for elastic response, it can be shown from numerical analysis (Davis & Rabinowitz, 1984) that $2n+1$ equally spaced integration points around the full circumference are necessary. It is noted that only half-circumference is analyzed because of the symmetry of cross-sectional deformation. In our case, Fourier series expansion of eighth degree is used. Consequently, the corresponding optimum number of integration points around entire circumference is 17 points, which make 9 points around the half-circumference. The numerical results verify that nine integration points around the half-circumference with provide very good results.

Finally, the stresses calculated from this finite element analysis are compared with the analytical solutions described in the Appendix, assuming linear elastic solution.

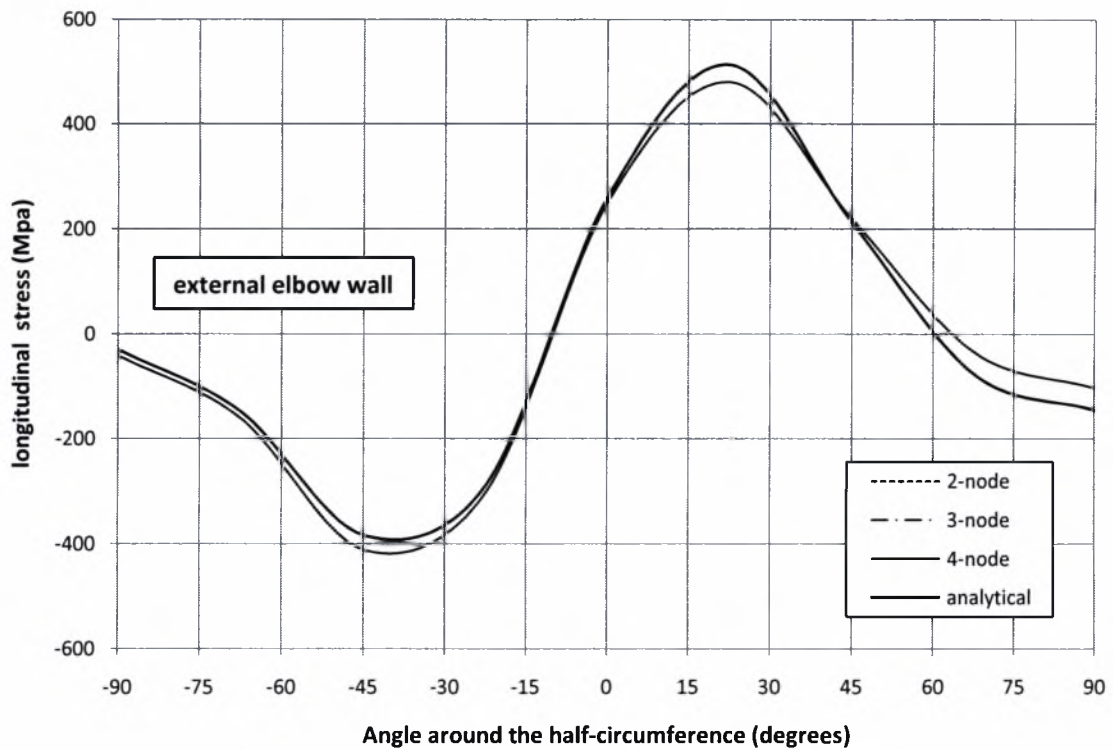


Figure 5: Variation of longitudinal stress at external elbow wall; comparison of analytical solution with numerical results

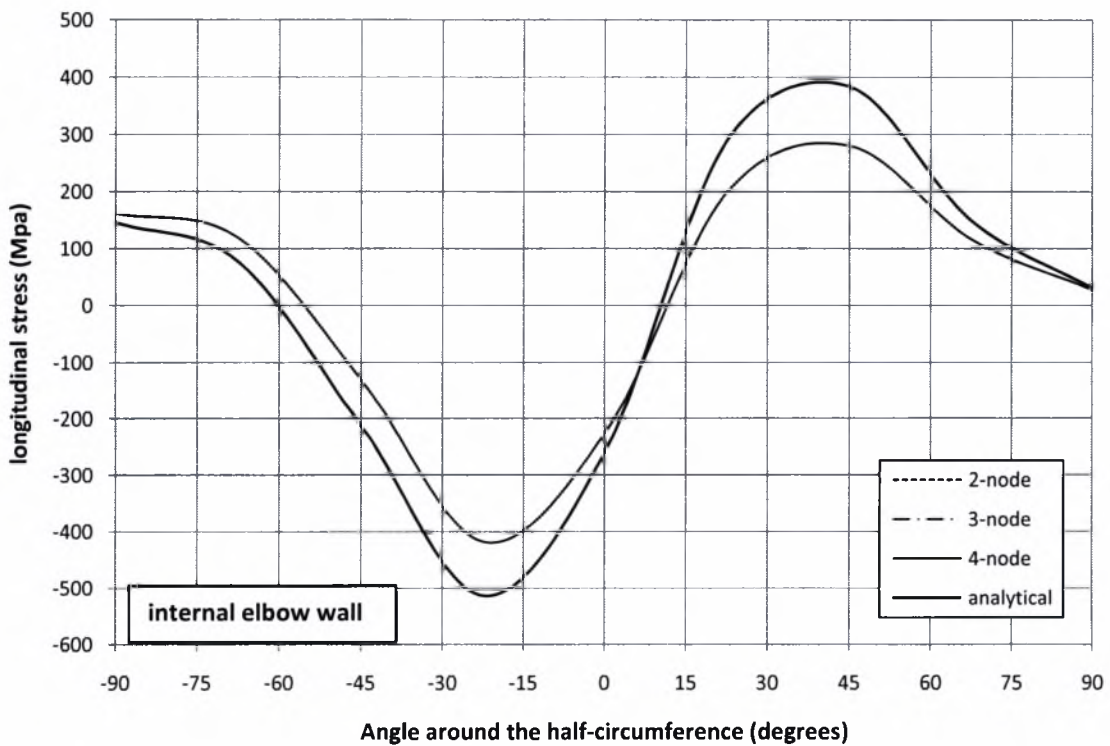


Figure 6: Variation of longitudinal stress at internal elbow wall; comparison of analytical solution with numerical results

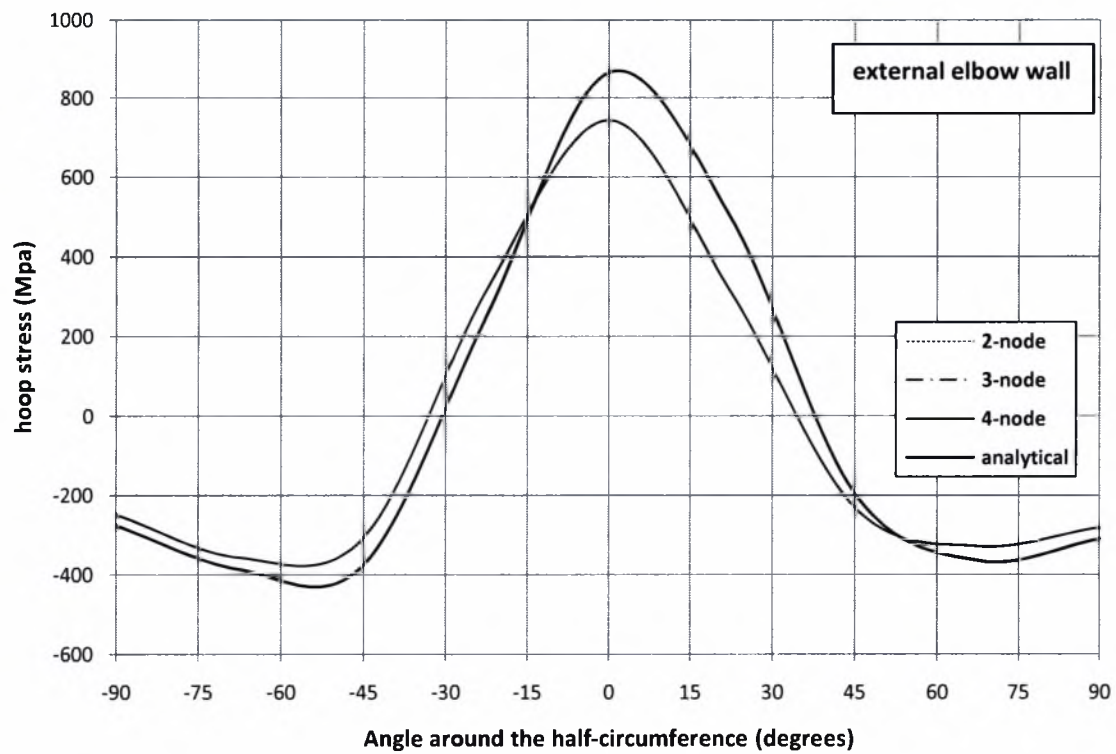


Figure 7: Variation of hoop stress at external elbow wall; comparison of analytical solution with numerical results

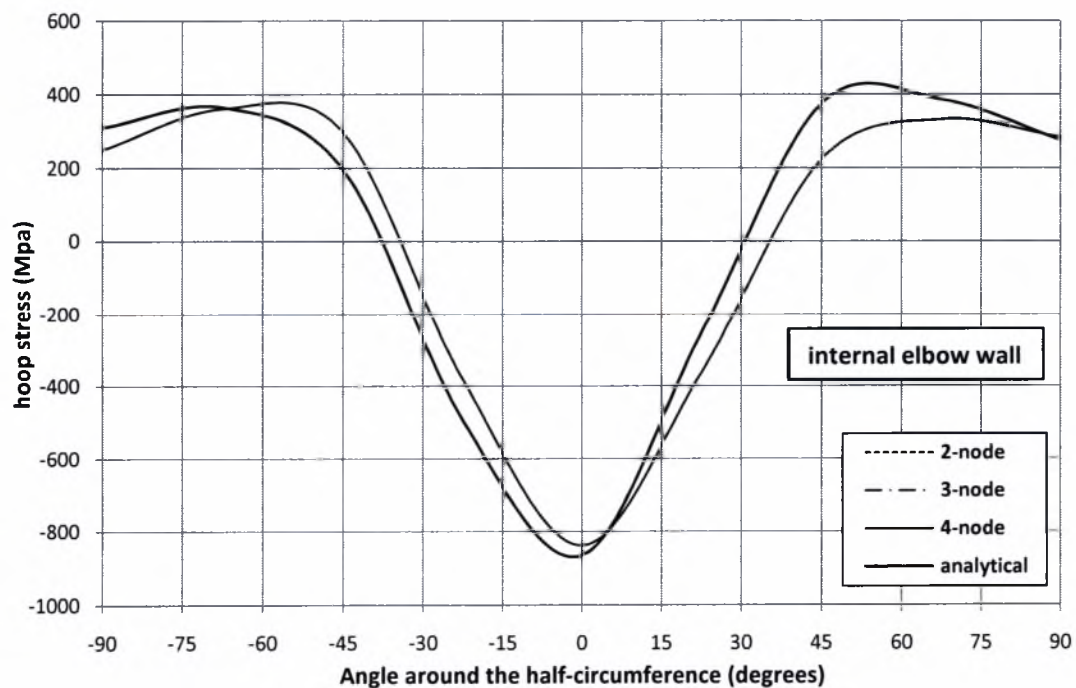


Figure 8: Variation of hoop stress at internal elbow wall; comparison of analytical solution with numerical results

The comparison is shown in Figure 5 and Figure 6 for the longitudinal stress around the elbow cross-section at external and internal elbow wall respectively. The maximum longitudinal stress is considerably higher than the maximum stress of a straight pipe with the same cross-section, and does not occur at the top or the bottom of the cross-section. The cross-sectional ovalization of the cross-section is mainly responsible for this behavior. Figure 7 and Figure 8 depict the hoop stress around the elbow cross-section at external and internal elbow wall respectively. It is interesting to note that the maximum circumferential stress is higher than the maximum longitudinal stress. It is noted that only half-circumference is analyzed because of the symmetry of cross-sectional deformation and the number of integration points are 9 around the half-circumference.

In general, the analytical and numerical results are in adequate agreement. The fact that the numerical and the analytical results do not agree precisely is due to that the numerical results are based in three-dimensional analysis in contrast with analytical results which are based in two-dimensional analysis. Also in the analytical solution, the radial and tangential displacements are discretized through series of doubly-symmetric trigonometric functions.

3.2 Element tests in a 90deg elbow

A parametric study is also conducted to investigate the response of a free standing 90 deg elbow under in-plane bending. The response of this initially curved tube (Figure 9) is analyzed with element of different number of nodes (2, 3 or 4). Similarly with the pipe considered in the previous analysis, the outside diameter is 165 mm, the thickness is 3 mm, and R/r ratio equal to 5.92. The applied bending moment is equal to 10 kN-m and, the material is steel with Young's modulus and Poisson's ratio are $E=210$ GPa and $\nu=0.3$ respectively. The elbow geometry is expressed in terms of the dimensionless elbow parameter λ .

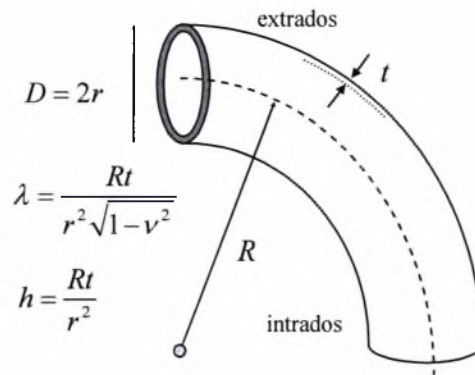


Figure 9: Pipe elbow geometry

Table 7 shows the normalized curvature and ovalization of the elbow, for parameter λ is equal to 0.23. The number of Fourier series expansion is eighth degree and the number of integration points is 9 points around the half-circumference, 1, 2 and 3 points for 2, 3 and 4 node "tube element" respectively, in the longitudinal direction and 3 points in the radial direction. The response of elbow is presented for the two-node "tube element" and parametric analysis is conducted for different number of elements, which are used to model the curved tube.

	Normalized curvature κ	Ovalization
1 element	0.036321	0.007348
2 elements	0.110024	0.029292
3 elements	0.135512	0.037101
4 elements	0.141166	0.038869
5 elements	0.142724	0.039366
10 elements	0.143600	0.039664
20 elements	0.143595	0.039671
100 elements	0.143575	0.039667
Analytical solution	0.143988	0.039820

Table 7: Normalized curvature and ovalization of elbow; comparison of analytical solution with numerical results, for 2-node "tube element"

Similarly, in tables 8 and 9 the normalized curvature κ and ovalization of the elbow for 3-node and 4-node “tube element” are presented respectively.

	Normalized curvature κ	Ovalization
1 element	0.143247	0.143247
2 elements	0.143561	0.039664
3 elements	0.143571	0.039666
4 elements	0.143573	0.039667
5 elements	0.143574	0.039667
10 elements	0.143574	0.039667
20 elements	0.143574	0.039667
Analytical solution	0.143988	0.039820

Table 8: Normalized curvature and ovalization of elbow; comparison of analytical solution with numerical results, for 3-node “tube element”

	Normalized curvature κ	Ovalization
1 element	0.143546	0.039647
2 elements	0.143576	0.039671
3 elements	0.143576	0.039669
4 elements	0.143575	0.039668
5 elements	0.143575	0.039668
10 elements	0.143574	0.039667
20 elements	0.143574	0.039667
Analytical solution	0.143988	0.039820

Table 9: Normalized curvature and ovalization of elbow; comparison of analytical solution with numerical results, for 4-node “tube element”

The numerical results show that for the 2-node “tube element”, at least 10 elements are needed for having convergence of solution. The convergence of solution for 3-node “tube element” is becoming with 5 elements and for 4-node “tube element”, 2 elements are enough. This is due to linear, quadratic or cubic polynomials which are used to the corresponding Lagrangian functions for each tube element type (2-node, 3-node, 4-node). The fact that the numerical and the analytical results do not agree precisely is due to the three-dimensional analysis of the numerical results in contrast with analytical results which are based in two-dimensional analysis.

Finally, it is noted that reduced integration is used in the longitudinal direction, i.e. 1, 2 and 3 points for 2, 3 and 4 node “tube element” respectively. The reason for using reduced integration is that the elements display much too stiff a behavior, for full integration in the longitudinal direction, i.e. 2, 3 and 4 points for 2, 3 and 4 node “tube element” respectively.

3.3 Element tests on an industrial piping component

The element tests clearly indicate the particular behavior of curved pipe, assuming elastic behavior and constant curvature along the pipe. However, in real industrial applications, elbows are connected to straight pipe segments, resulting in a variation of deformation along the elbow. In this paragraph, a parametric study is described aimed at investigating the bending response of a 90 deg elbow and two straight parts of length equal to six pipe diameters (990 mm) under in-plane bending (Figure 10). Only half of specimen is considered (A-F), with symmetry conditions in section F (Figure 10). The opportune boundary conditions are applied in end-section A, which is considered, undeformed. Moment is applied at the end section A. A total of 24 tube elements are used, with 8th degree expansion.

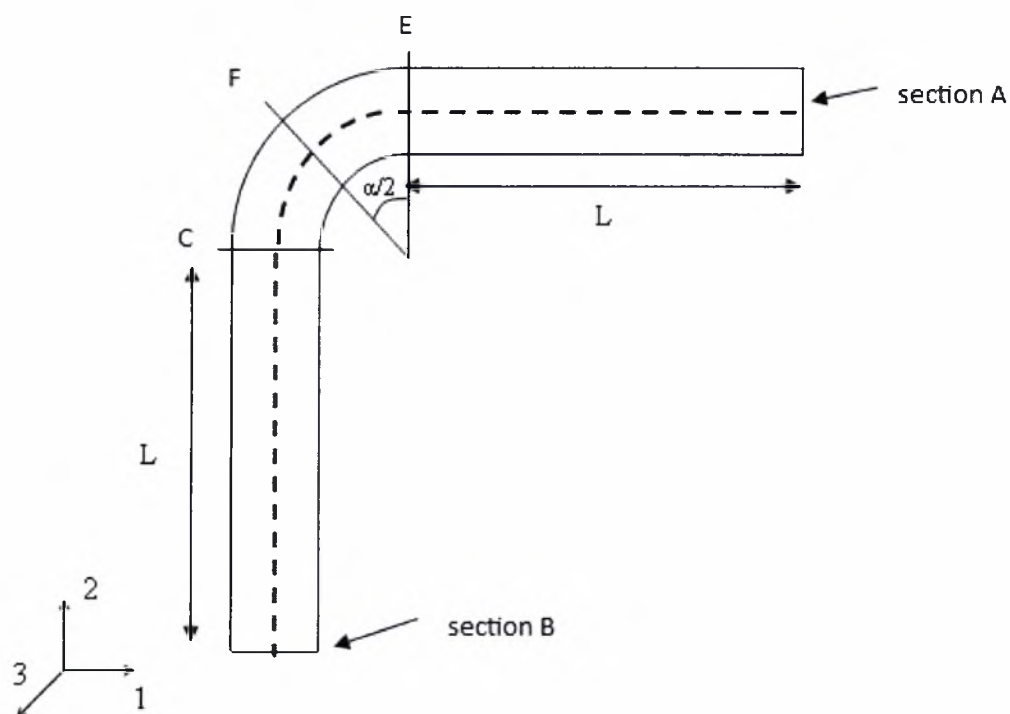


Figure 10: Specimen geometry

Comparison	Normalized curvature κ	Ovalization
2-node "tube element"	0.131995	0.041498
3-node "tube element"	0.132123	0.041539
4-node "tube element"	0.132121	0.041539
shell element - Abaqus	0.138228	0.041683
Analytical solution	0.143988	0.039820

Table 10: Normalized curvature and ovalization of elbow; comparison between analytical and numerical results

In Table 10 shows the comparison between the numerical results for 2, 3 and 4 node “tube element” and the analytical results. Also, the results of analysis with shell element of Abaqus are presented. The normalized curvature is defined as

$$k = \frac{\varphi_{CE}}{L} \quad (3.4)$$

where φ_{CE} is the relative rotation between the cross-sections C and E, the ends of the curved pipe segment (Table 10) and $L = R \frac{\pi}{2}$ (because of 90 deg elbow) and is normalized by the curvature-like parameter $k_N = t / (r^2 \sqrt{1 - \nu^2})$, so that $\kappa = k / k_N$. Due to symmetry with respect to middle section F, $\varphi_{CE} = \varphi_E$. The rotation of a cross-section is determined from the value of the rotational DOF of the corresponding tube element node. The ovalization of elbow is expressed in terms of the ovalization parameter (equation 3.2), where D_h and D_v are the deformed lengths of the horizontal diameter (normal to the plane of bending) and of the vertical diameter (on the plane of bending) in section F.

Furthermore, this specimen is analyzed with shell elements (type S4R) of Abaqus. The rotation of cross-section E is calculated from the relative displacements of two nodes on this section, similarly the rotation of cross-section C is calculated from the respectively relative displacements of two nodes on that section. The relative rotation between the cross-sections C and E is the sum of these rotations.

The analytical solution is based in two-dimensional analysis, so the differences in the comparison between the numerical results and the analytical results are expected. Also, the differences in the results are attributed to the adjacent straight parts.

Finally, Figures 11, 12 and 13 show the variation of ovalization along the pipe length, for 2, 3 and 4 node “tube element”. The curved pipe is divided in three parts, the first part is the straight pipe, the second part is the 40 deg part from E section and the third part is 5 degrees from F section. For the analysis, 5, 10 and 20 tube

elements are used. Especially, for the analysis with 5 elements, 2 elements are used in first part, 2 in the second and 1 in the last part of elbow pipe. Respectively for the analysis with 10 elements, 2-4-4 elements are used in each part and for analysis with 20 elements 6-7-7 elements are used in each part respectively. The maximum ovalization is in section F, and in the straight parts of tube the ovalization is equal to zero.

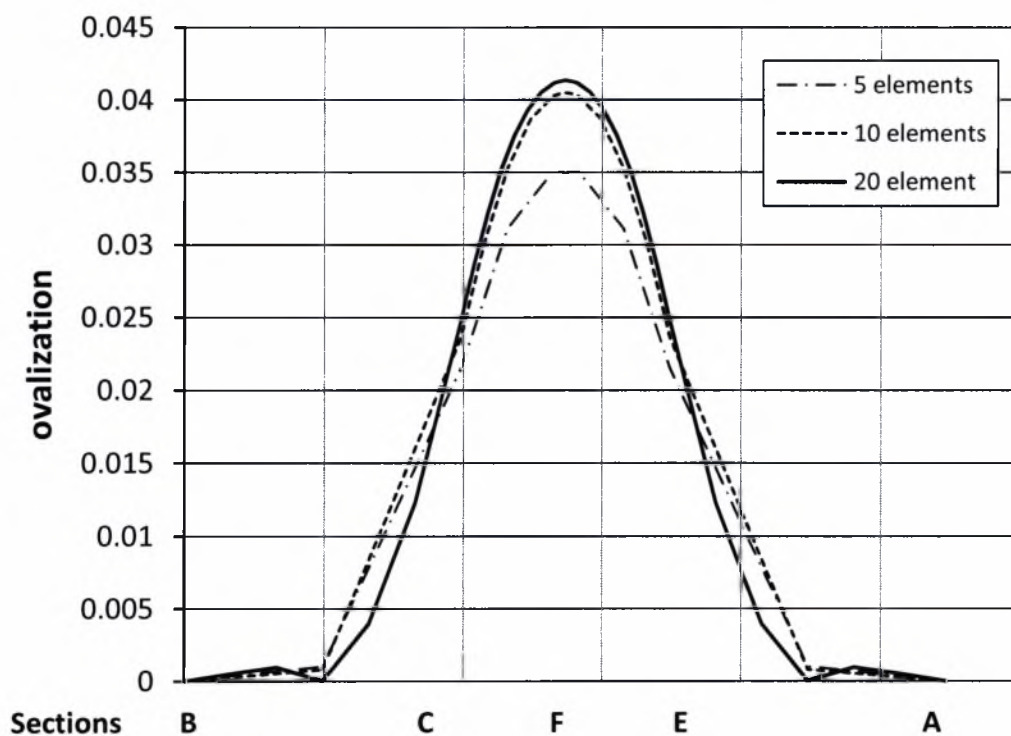


Figure 11: Variation of ovalization along the pipe length; for 2- node “tube element”

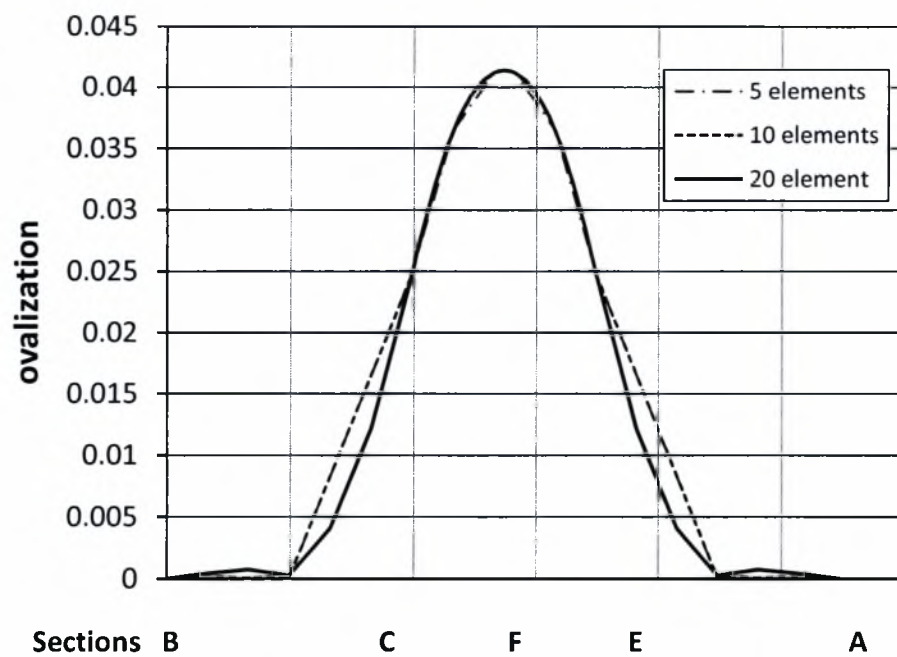


Figure 12: Variation of ovalization along the pipe length; for 3- node "tube element"

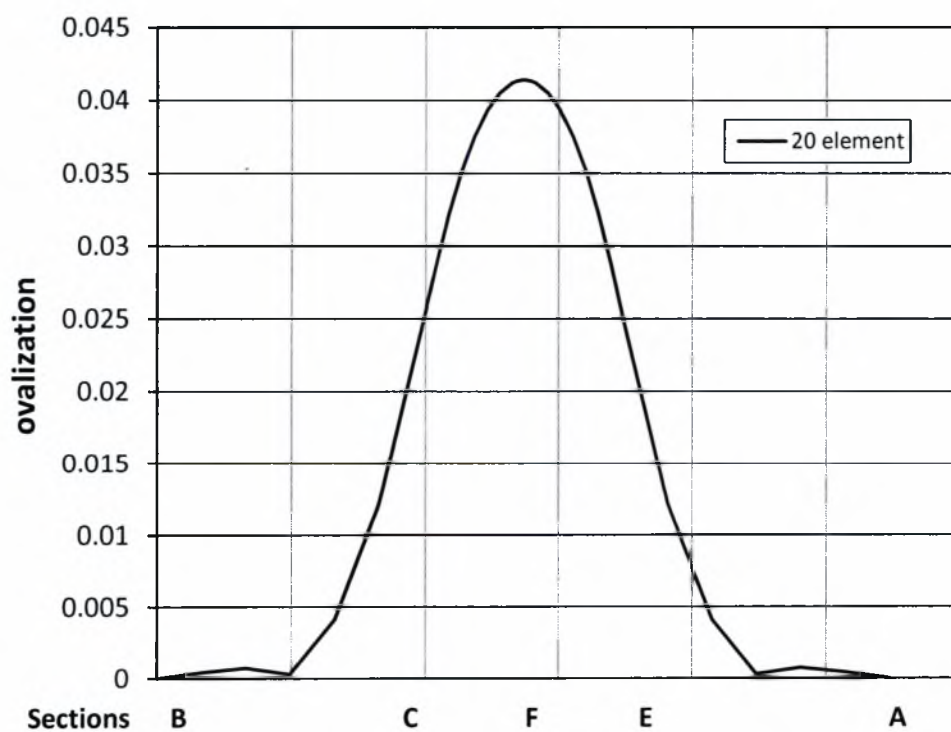


Figure 13: Variation of ovalization along the pipe length; for 4- node "tube element"

Chapter 4

Numerical Results – Comparison with Experiments

In this chapter, numerical results for relatively elastic elbows are obtained, and compared with experimental data, conducted at TNO, the Netherlands. The work is based on simulation of elastic elbows with “tube elements”, presented and tested in previous chapters. A part from comparing our numerical results with test data, the present study is aimed at elucidating some interesting parts of elbow mechanical behavior.

The numerical results are compared with experimental measurements from a 30 deg and 60 deg steel elbows under in-plane bending (Figure 14). The test specimens consisted of moderately thin-walled elbows ($\varnothing 160$ -2.9 mm, $D/t=55$) and thin-walled elbows ($\varnothing 261$ -2.9 mm, $D/t=90$). Each specimen consisted of a curved middle part connected to two straight parts; the length of each straight part is equal to 1200 mm, and a curved part, corresponding to an angle of 30 deg or 60 deg. The straight parts of the pipe had the same outer diameter and a slightly different thickness (3 mm). Young’s modulus and Poisson’s ratio are $E=210$ GPa and $\nu=0.3$ respectively.

In our simulation, only half of each specimen is considered (A-F), with symmetry conditions in section F. End section A is considered underformed, free to move horizontally, but restrained in the vertical direction. Moment is applied at the end section A. the results focus on the relative rotation ϕ_{CE} between cross-section C and E, the ends of the curved pipe segment , as well as the cross-sectional ovalization in section F.

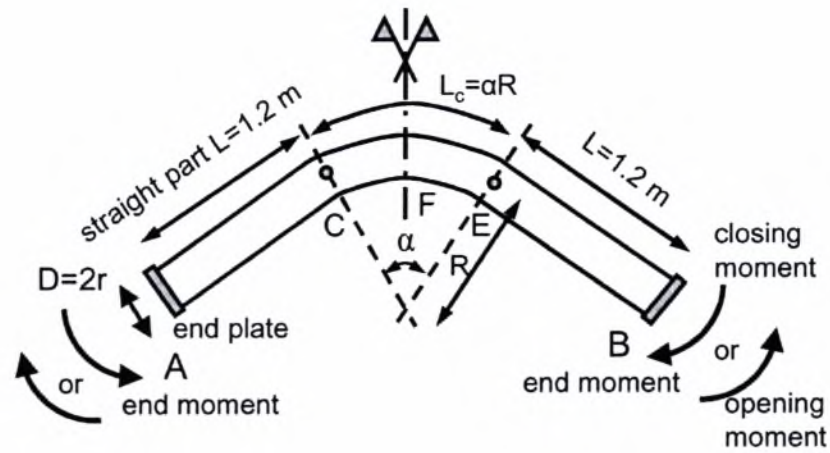


Figure 14: Specimen geometry

4.1 Comparison with TNO experimental results

A series of steel elbow experiments were conducted in TNO (Gresnigt et al. 1985), which were aimed at examining the response of elbows ($R/r=6$) under in-plane bending (opening and closing end moments). Those tests are used for comparison with numerical results in the present work.

Specimen No.	D (mm)	t (mm)	R (mm)	Angle α (deg)	Bending type
70	160	2.9	480	30	closing
71	160	2.9	480	30	opening
72	160	2.9	480	30	closing
73	160	2.9	480	30	opening
81	261	2.9	772	60	closing
82	261	2.9	772	60	opening
83	261	2.9	772	60	closing
84	261	2.9	772	60	opening

Table 11: Elbow specimens tested at TNO

Each specimen was tested under in-plane bending (opening and closing bending moments were considered) (table 11). Bending moment is plotted in terms of the relative rotation ϕ_{CE} between cross-sections C and E, the ends of the curved pipe segment (Figure 14). Obviously, due to linear analysis, the moment –rotation curve is a straight line. Due to symmetry with respect to the middle section F, $\phi_{CE}=2\phi_C$. Figures 15 and 16 show the comparison of the experimental moment-rotation ($M-\phi_{CE}$) curves with the corresponding numerical results for relatively-thick-walled specimens 70 and 71. In specimens 70 and 71, there is a considerable difference between the experimental data and the numerical results.

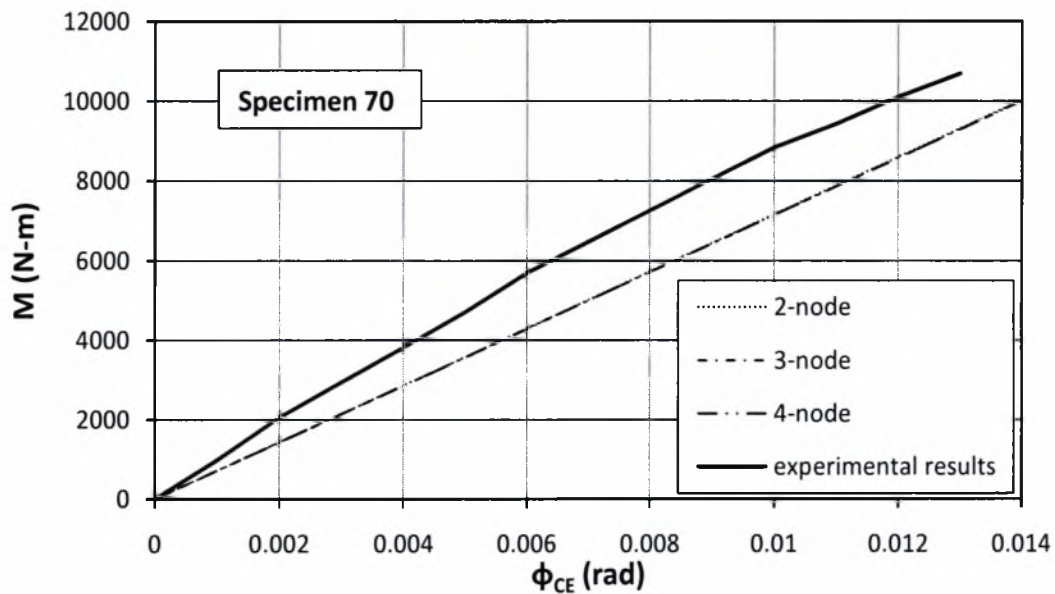


Figure 15: Moment-rotation paths for specimen 70; comparison between test data and numerical results.

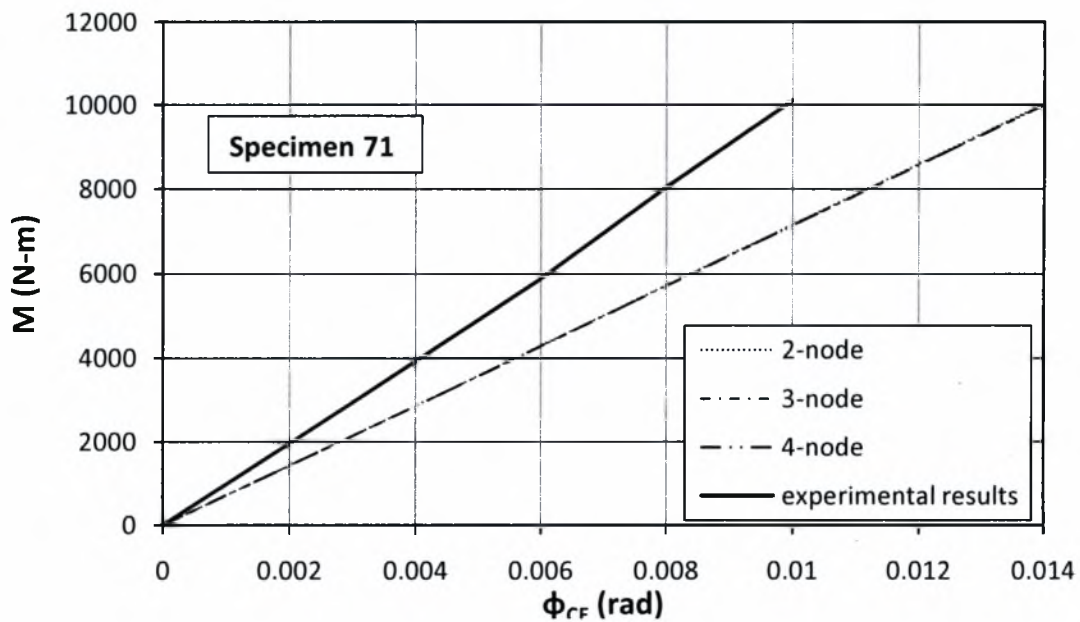


Figure 16: Moment-rotation paths for specimen 71; comparison between test data and numerical results

Furthermore, Figure 17 and Figure 18 show the comparison of the experimental moment-rotation (M - ϕ_{CE}) curves with the corresponding numerical results for specimens 72 and 73. The comparison with specimen 72 is very good, but there is a rather poor comparison with specimen 73.

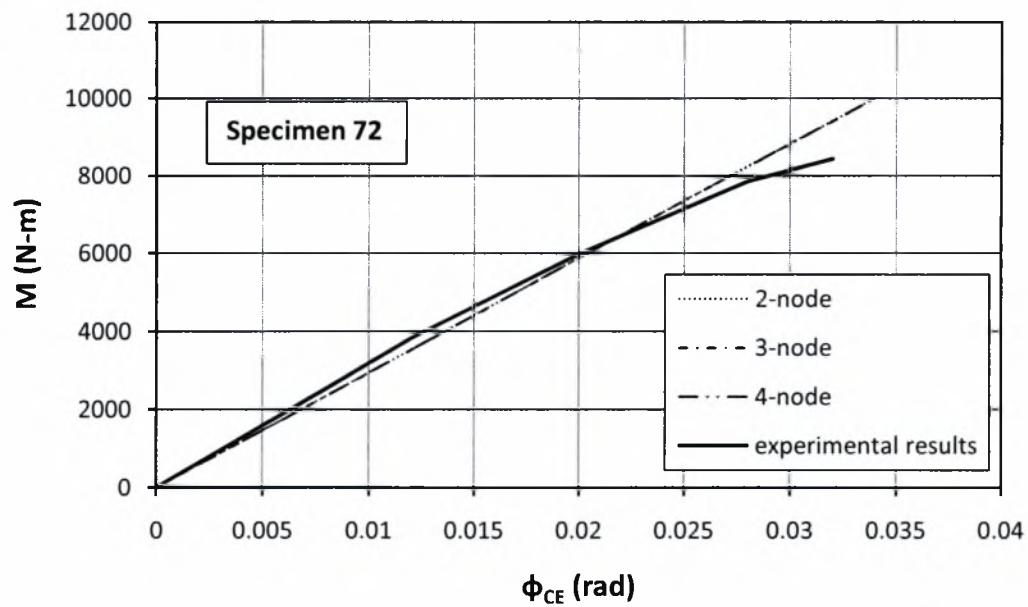


Figure 17: Moment-rotation paths for specimen 72; comparison between test data and numerical results

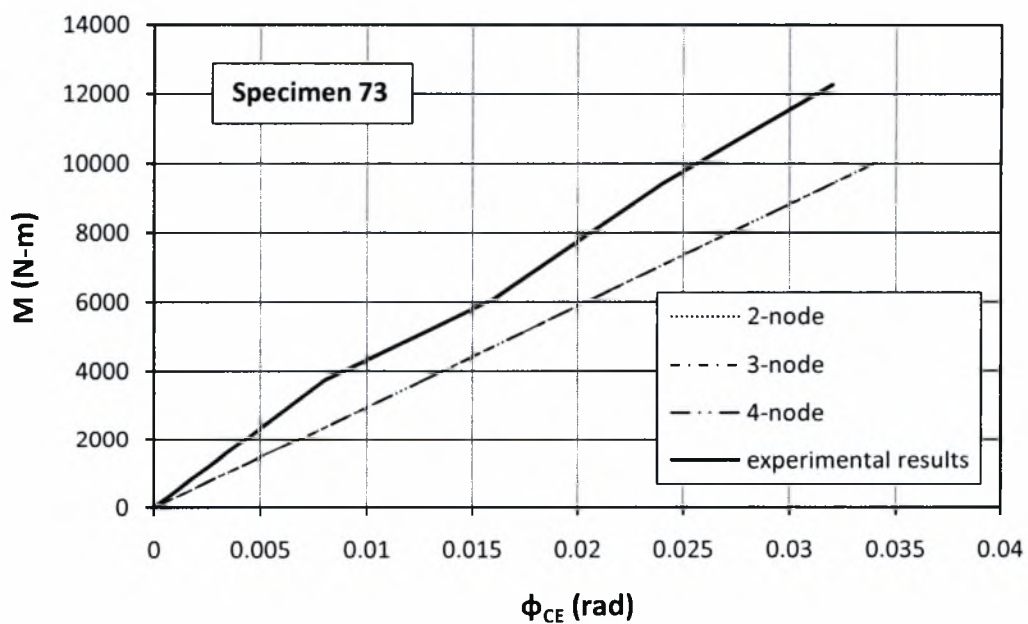


Figure 18: Moment-rotation paths for specimen 73; comparison between test data and numerical results

Figure 21 to Figure 24 show the comparison of the experimental moment-rotation ($M-\phi_{CE}$) curves with the corresponding numerical results for specimens 81, 82, 83 and 84. In specimens 81 and 82, there is a considerable difference between the experimental data and the numerical results. This difference is less pronounced in specimens 83 and 84.

To explain this difference, it is important to point out that the rotation of a cross-section is defined in experiments differently than in tube element analysis. Experimentally, it is measured through the rotation of the steel frames attached to the elbow at the mid-height of the cross-section (Figure 19, Figure 20). In the tube element analysis, the rotation of the cross-section is determined from the value of the rotational DOF of the corresponding tube element node.

In this point, note that specimens 70 and 71 have a small curved part, so that the pipe cross-section exhibits significant warping at C. This effect is alleviated in specimens 72 and 73, because the curved pipe portion is significantly longer. In other words, section C of specimens 72 and 73, exhibits less warping deformation and this accounts for the fairly good comparison between experimental and numerical values of initial stiffness. Similarly, the specimens 81 and 82 have smaller curved part than the specimens 83 and 84, so the difference is less pronounced in specimens 83 and 84.

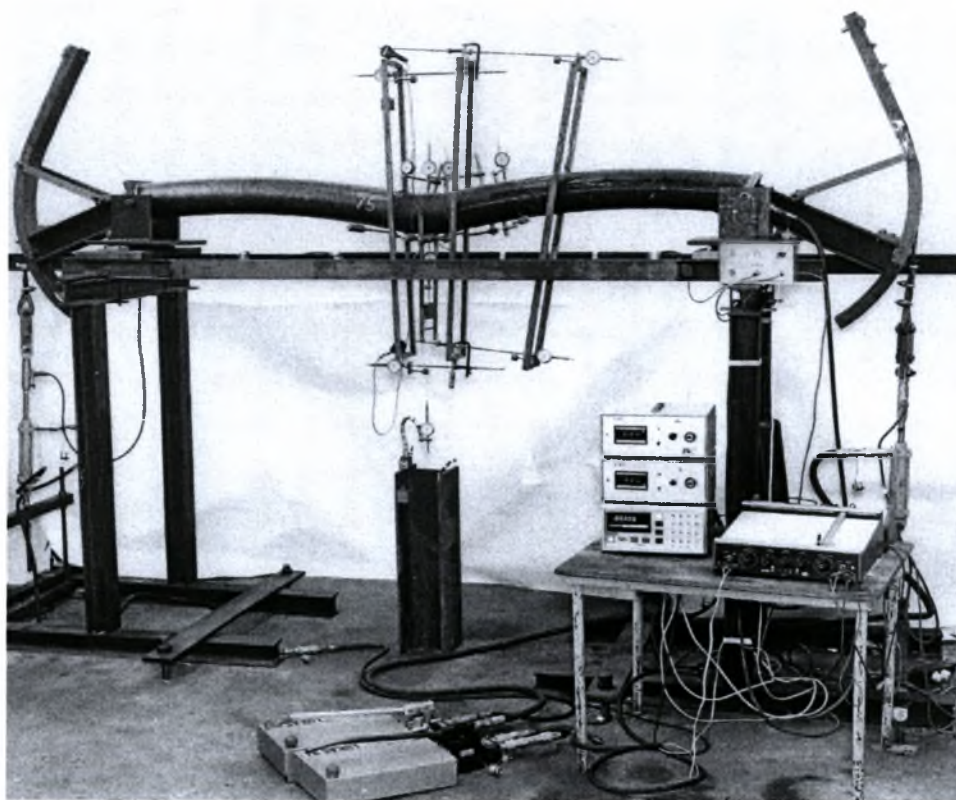


Figure 19: Experimental set-up for specimens, tested at TNO

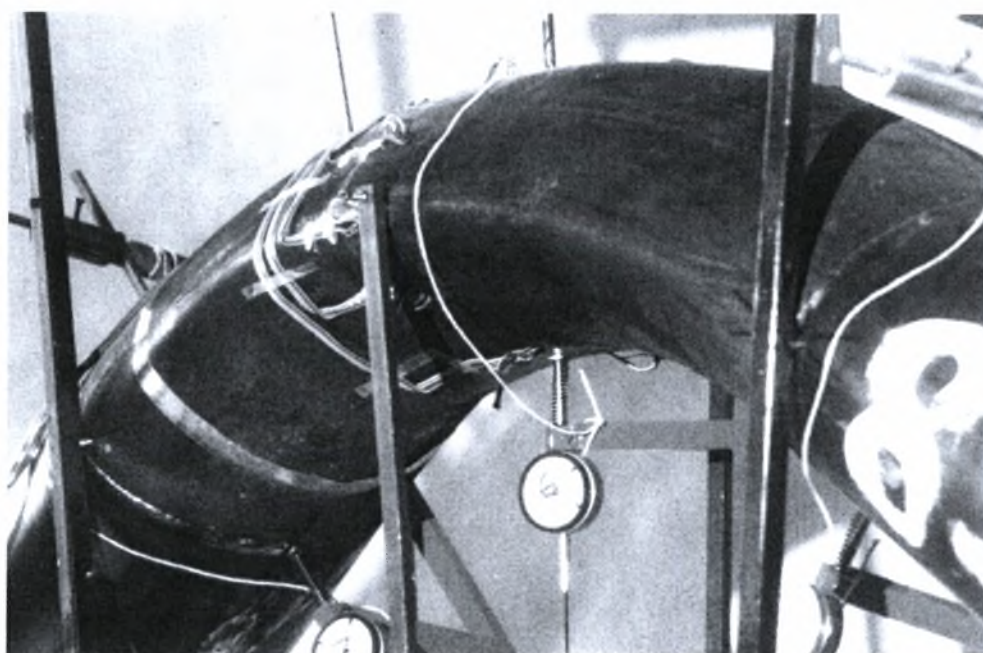


Figure 20: Devices for measuring rotations and ovalization in specimens

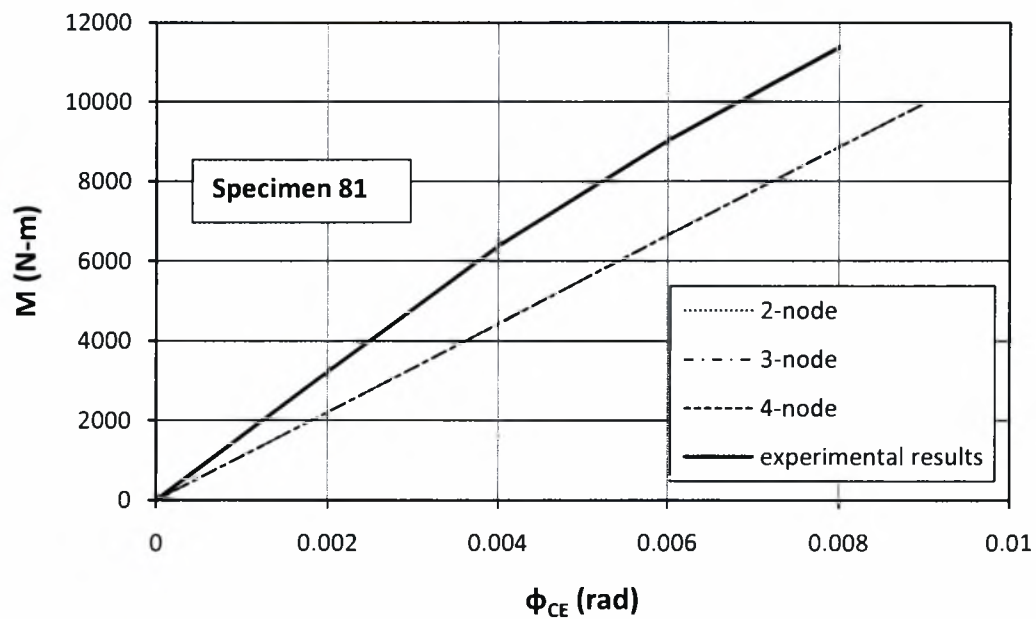


Figure 21: Moment-rotation paths for specimen 81; comparison between test data and numerical results

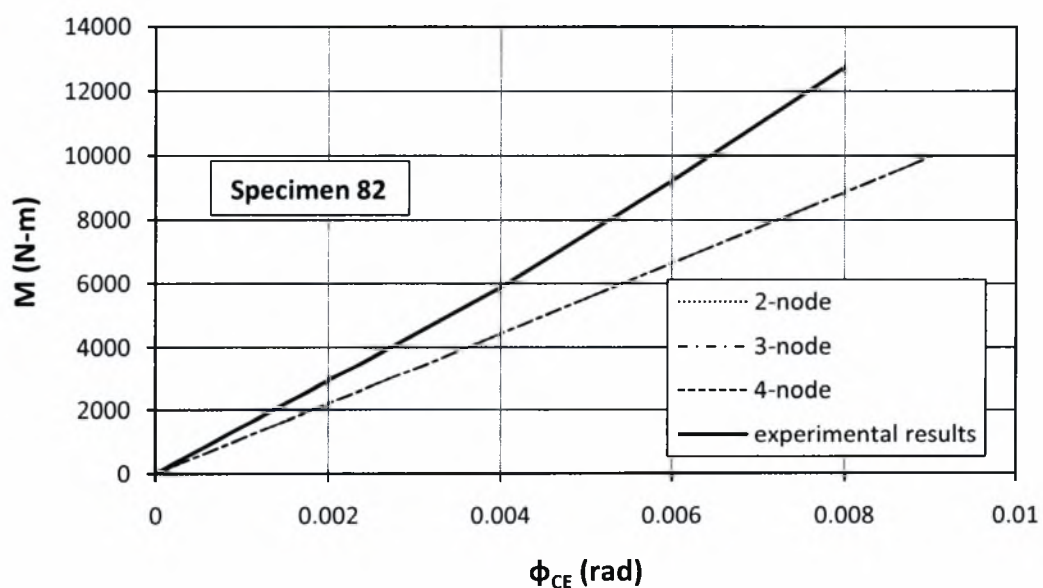


Figure 22: Moment-rotation paths for specimen 82; comparison between test data and numerical results

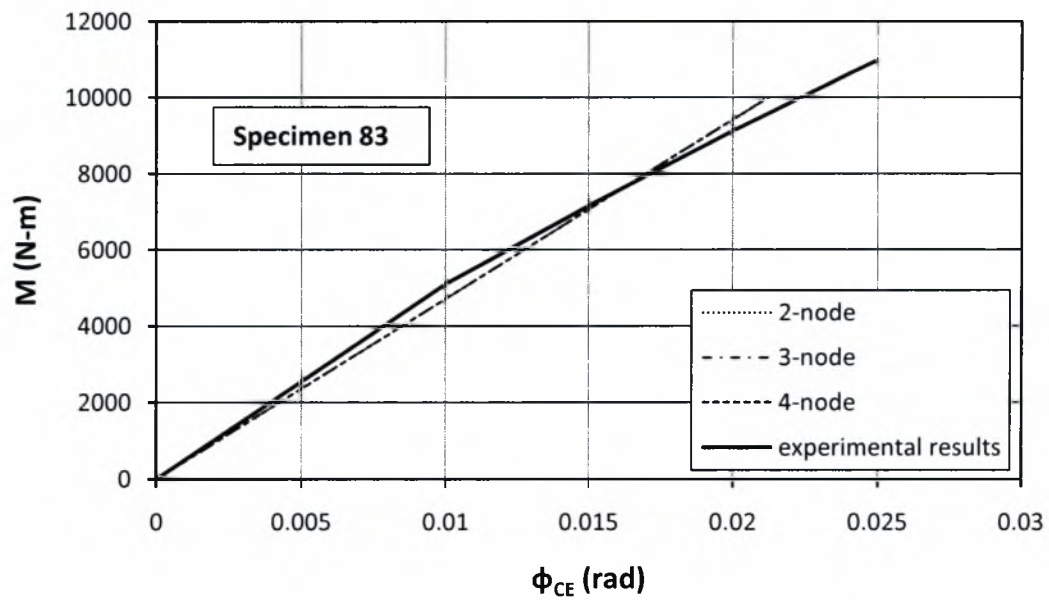


Figure 23: Moment-rotation paths for specimen 83; comparison between test data and numerical results

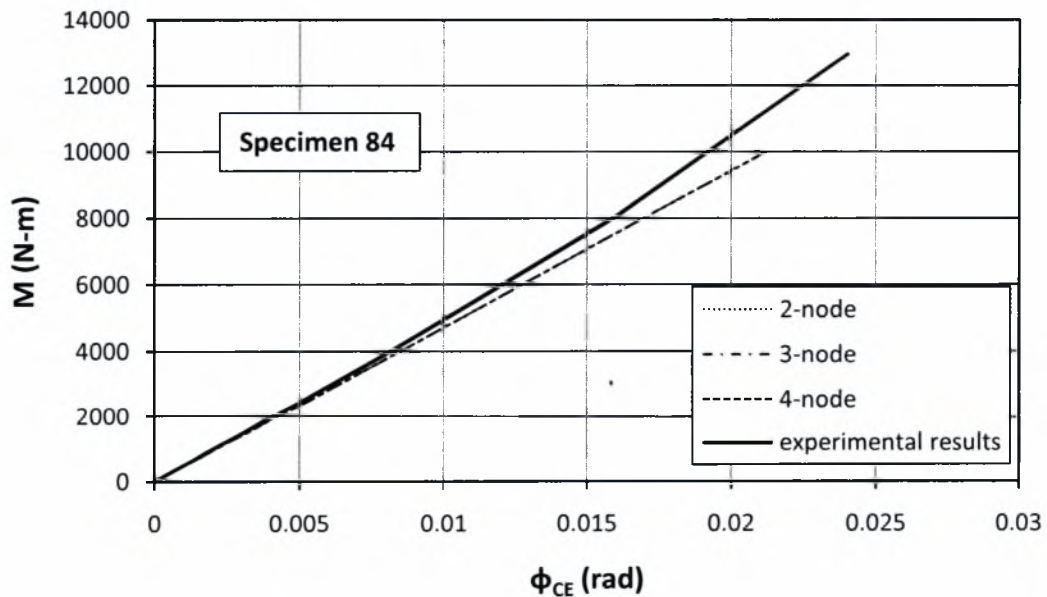


Figure 24: Moment-rotation paths for specimen 84; comparison between test data and numerical results

Chapter 5

Conclusions

A linear finite element, referred to as a “tube element”, was developed for the purposes of this research. The present work was motivated by the desire for optimum behavior of the proposed “tube element family” (2-node, 3-node, 4-node). Several benchmark problems were considered towards this purpose. The basic issues examined were the optimum number of the cross-sectional parameters and the corresponding number of integration points in the three directions. Comparisons were made with the analytical solution, in terms of pipe deformations and stresses.

In the final part of this study, the numerical technique was employed to analyze 30 deg and 60 deg steel elbows under in-plane bending. The numerical results were compared with experimental data, conducted at TNO. The work was based on simulation of elastic elbows with “tube element”.

The present study was aimed at providing optimum behavior of the proposed “tube element family” (2-node, 3-node, 4-node). However, further numerical results are necessary in the area of elbows in the presence pressure and under out-of-plane bending.

Appendix

Analytical Linear Solution

A simplified variational formulation has been proposed by Rodabaugh & George (1957) for the analysis of pressurized pipe linear elastic elbows under bending, in the presence of pressure. This formulation is presented briefly for the sake of completeness, and is based on the minimization of total potential energy, which equal to

$$\Pi = (U_L + U_C) - U_2 - M \cdot k \quad (1.1)$$

The strain energy is the sum of the longitudinal strain energy U_L and the hoop strain energy U_C . Expressing the longitudinal and the hoop strain are expressed in terms of the radial and tangential displacements of the cross-section

$$\varepsilon_L = \frac{1}{R} \left(\frac{\Delta\alpha}{\alpha} r \sin \varphi + v \cos \varphi + w \sin \varphi \right) \quad (1.2)$$

$$\varepsilon_c = \frac{1}{r^2} \left(\frac{d^3 v}{d\varphi^3} + \frac{dv}{d\varphi} \right) \zeta \quad (1.3)$$

where α and $\Delta\alpha$ are the elbow angle and change of elbow angle respectively, the longitudinal strain energy and the hoop strain energy can be written as follows

$$U_L = \frac{Etr}{2R^2} \int_0^{2\pi} \left(\frac{r\Delta\alpha}{\alpha} \sin \varphi + v \cos \varphi + w \sin \varphi \right)^2 d\varphi \quad (1.4)$$

$$U_C = \frac{1}{2} \frac{Er}{(1-\mu^2)} \int_{A_0} \varepsilon_\theta^2 d\theta d\rho = \frac{Et^3}{24(1-\mu^2)r^3} \int_0^{2\pi} (v' + v''') d\theta \quad (1.5)$$

A Galerkin discretization of the displacements is assumed in terms of doubly-symmetric trigonometric functions

$$v = \sum_{n=1}^{\infty} a_n \sin 2n\varphi \quad (1.6)$$

$$w = -\sum_{n=1}^{\infty} 2a_n \cos 2n\varphi \quad (1.7)$$

Inserting those expressions into the strain energy expression, one obtains

$$U_1 = \frac{Etr}{2R^2} \left\{ \int_0^{2\pi} \left(\frac{r\Delta\alpha}{\alpha} \sin \varphi + \cos \varphi \sum_{n=1}^{\infty} a_n \sin 2n\varphi - \sin \varphi \sum_{n=1}^{\infty} 2a_n \cos 2n\varphi \right)^2 d\varphi \right. \\ \left. + \frac{\lambda^2}{12} \int_0^{2\pi} \left(-\sum_{n=1}^{\infty} 8n^3 a_n \cos 2n\varphi + \sum_{n=1}^{\infty} 2na_n \cos 2n\varphi \right)^2 d\varphi \right\} \quad (1.8)$$

Furthermore, the work conducted by the pressure should be considered. This is equal to the product of pressure and the change of area enclosed by the pipe cross-section ($U_2 = P\Delta A$). It can be shown that, using the discretization expressed in equations, the following expression is obtained:

$$U_2 = -2\pi P \sum_{n=1}^{\infty} n^2 (4n^2 - 1) a_n^2 \quad (1.9)$$

Therefore, the total potential energy is expressed as follows:

$$\Pi = \frac{Etr\pi}{2R^2} \left\{ r^2\eta^2 + 3r\eta a_1 + \frac{9}{4}a_1^2 + \frac{1}{4} \sum_{n=1}^{\infty} \left[a_n(1-2n)^2 - 2a_n a_{n+1}(2n-1)(2n+3) + a_{n+1}^2(2n+3)^2 \right] + \frac{\lambda^2}{12} \sum_{n=1}^{\infty} a_n^2(8n^3-2n)^2 + 4\psi \sum_{n=1}^{\infty} n^2(4n^2-1)a_n^2 \right\} - Mk \quad (1.10)$$

where $\eta = \Delta\alpha/\alpha$. Minimization of the above expression in terms of a_i , results in a system of linear equations in terms of a_i , which can be readily solved. Upon calculation of the solution, $\eta = \Delta\alpha/\alpha$ is calculated as follows:

$$\eta = \frac{MR}{EI} \left\{ 1 + 3d_1 + \frac{9}{4}d_1^2 + \frac{1}{4} \sum_{n=1}^{\infty} \left[d_n(1-2n)^2 - 2d_n d_{n+1}(2n-1)(2n+3) + d_{n+1}^2(2n+3)^2 \right] + \frac{\lambda^2}{12} \sum_{n=1}^{\infty} d_n^2(8n^3-2n)^2 + 4\psi \sum_{n=1}^{\infty} n^2(4n^2-1)d_n^2 \right\}^{-1} \quad (1.11)$$

where $d_n = a_n / r\eta$. In a straight beam,

$$\eta_0 = \frac{MR}{EI} \quad (1.12)$$

The flexibility factor for curved pipe is expressed as follows

$$k = \frac{\eta}{\eta_0} \quad (1.13)$$

The longitudinal and hoop strains are computed as follows

$$\varepsilon_L = \frac{1}{R} \left(\frac{\Delta\alpha}{\alpha} r \sin \varphi + \cos \varphi \sum_{n=1}^{\infty} a_n \sin 2n\varphi - \sin \varphi \sum_{n=1}^{\infty} 2a_n \cos 2n\varphi \right) \quad (1.14)$$

$$\varepsilon_c = \pm \frac{t}{2r^2} \left(\sum_{n=1}^{\infty} 8n^3 a_n \sin 2n\varphi - \sum_{n=1}^{\infty} 2na_n \sin 2n\varphi \right) \quad (1.15)$$

Finally, the corresponding stresses are computed from Hooke's law as follows

$$\sigma_L = \frac{E}{1-\nu^2} (\varepsilon_L + \nu \varepsilon_C) \quad (1.16)$$

$$\sigma_C = \frac{E}{1-\nu^2} (\varepsilon_C + \nu \varepsilon_L) \quad (1.17)$$

References

- Bathe, K. J. and Almeida, C. A., 1980, "A simple and effective pipe elbow element – Linear analysis", J. Applied Mechanics, ASME, Vol. 47, pp.93-100.
- Bathe, K. J. and Almeida, C. A., 1982, "A simple and effective pipe elbow element – Interaction effects", J. Applied Mechanics, ASME, Vol. 49, pp.165-171.
- Brazier, L. G., 1927, "On the flexure of thin cylindrical shells and other "thin" sections", Proceedings of the Royal Society, series A, Vol. 116, pp. 104-114.
- Brush D.O., Almroth, B.O., 1975, "Buckling of bars, plates and shells", McGraw Hill, New York, NY.
- Davis J. P. and Rabinowitz P., 1984, "Methods of Numerical Integration", Academic Press, London.
- Dhalla, A. K., 1987, "Collapse Characteristics of a Thin-Walled Elbow", J. Pressure Vessel Technology, ASME, Vol. 109, pp. 394-401.
- Dodge W. G. and Moore S. E., 1972, "Stress indices and flexibility factors for moment loadings on elbows and curved pipes". Weld. Res. Cows. Bull. 197.
- Gresnigt, A. M. et al., 1985, "Preofresultaten van Proeven op Gladde Bochten en Vergelijking Daarvan met de in OPL 85-333 Gegeven Rekenregels", [in Dutch], Institute for Construction Materials and Structures, TNO-IBBC, Report OPL 85-334, Delft, The Netherlands.
- Gresnigt, A. M., 1986, "Plastic Design of Buried Steel Pipelines in Settlement Areas", Heron, Vol. 31, No. 4, Delft, The Netherlands.
- Gresnigt, A. M. and van Foeken, 1995, "Strength and Deformation Capacity of Bends in Pipelines", Int. J. Offshore and Polar Engineering, Vol. 5, No. 4, pp. 294-307.
- Hibbit, H. D., Karlsson and Sorensen, 2008, ABAQUS Theory Manual version 6.7, Hibbit, Karlsson and Sorensen Inc., Providence, RI.

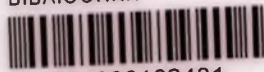
- Hilsenkopf, P., Boneh, B. and Sollogoub, P., 1988, "Experimental Study of Behavior and Functional Capability of Ferritic Steel Elbows and Austenitic Stainless Steel Thin-Walled Elbows". *Int. J. Pressure Vessels and Piping*, Vol. 33, pp. 111-128.
- Karamanos, S. A., Giakoumatos, E. and Gresnigt, A. M., 2003, "Nonlinear Response and Failure of Steel Elbows Under In-Plane Bending and Pressure", *J. Pressure Vessel Technology*, ASME, Vol. 125, No. 4, pp. 393-402.
- Karamanos, S. A. and Tassoulas, J. L., 1996, "Tubular Members I: Stability Analysis and Preliminary Results", *J. Engineering Mechanics*, ASCE, Vol. 122, No. 1, pp.64-71.
- Karamanos, S. A., Tsouvalas, D. and Gresnigt, A. M., 2006, "Ultimate Bending Capacity and Buckling of Pressurized 90 deg Steel Elbows.", *Journal of Pressure Vessel Technology*, ASME, Vol. 128, No. 3, pp. 348-356.
- Millittelo, C. and Huespe, A. E., 1988, "A displacement-based pipe elbow element", *Computers and Structures*, Vol. 29, No.2, pp. 339-343.
- Rodabaugh, E. C., and George, H. H., 1957, "Effect of internal pressure on the flexibility and stress intensification factors of curved pipe or welding elbows", *Transactions of the ASME* Vol. 79, pp.939-948.
- Sobel, L. H. and Newman, S. Z., 1980, "Comparison of Experimental and Simplified Analytical Results for the In-Plane Plastic Bending and Buckling of an Elbow", *J. Pressure Vessel Technology*, ASME, Vol. 102, pp. 400-409.
- Sobel, L. H. and Newman, S. Z., 1986, "Simplified, Detailed and Isochronous Analysis and Test Results for the In-Plane Elastic-Plastic and Creep Behavior of an Elbow", *J. Pressure Vessel Technology*, ASME, Vol. 108, pp. 297-304.
- Suzuki, N. and Nasu, M., 1989, "Non-Linear Analysis of Welded Elbows Subjected to In-Plane bending", *Computers and Structures*, Vol. 32, No.3/4, pp. 871-881.
- Tan, Y., Matzen, V. C. and Yu, L. X., 2002, "Correlation of test and FEA results for the nonlinear behavior of straight pipes and elbows", *J. Pressure Vessel Technology*, ASME, Vol. 124, pp. 465-475.
- Vigness, I., 1943, "Elastic Properties Of Curved Tubes", *Trans, ASME*, 65, pp.105-120.

Von Karman, Th., 1911, "Über die formänderung dünnwandiger Rohre, insbesondere federnder Ausgleichrohre", Z. Ver. Deutsch. Ingen., 55, pp. 1889-1895.

Yan, A. M., Jospin, R. J. and Nguyen, D. H., 1999, "An enhanced pipe elbow element – Application in plastic limit analysis of pipe structures", International Journal For Numerical Methods in Engineering, Vol. 46, pp. 409-431.



ΠΑΝΕΠΙΣΤΗΜΙΟ ΘΕΣΣΑΛΙΑΣ
ΒΙΒΛΙΟΘΗΚΗ



004000102431



ΣΥΓΓΡΑΦΕΑΣ

ΤΙΤΛΟΣ

ΛΗΞΗ

ΟΝΟΜΑΤΕΠΩΝΥΜΟ ΔΑΝΕΙΖΟΜΕΝΟΥ

13-5-11

ΠΑΝΕΠΙΣΤΗΜΙΟ ΘΕΣΣΑΛΙΑΣ
ΒΙΒΛΙΟΘΗΚΗ
Τηλ.: 24210 06300-1



